POSTMORTEM TIMING OF MICROBE-DRIVEN DECOMPOSITION EVENTS:

INDICATORS OF BLOAT AND POST-BLOAT IN CENTRAL TEXAS

by

Susan N. Sincerbox, B.S.

A thesis submitted to the Graduate Council of
Texas State University in partial fulfillment
of the requirements for the degree of
Master of Arts
with a Major in Anthropology
August 2018

Committee Members:

Michelle D. Hamilton, Chair

Daniel J. Wescott

Nicholas P. Herrmann

J.P. Fancher

FAIR USE AND AUTHOR'S PERMISSION STATEMENT

Fair Use

Duplication Permission

ACKNOWLEDGEMENTS

I would first like to thank the past, present, and future donors to the Willed Body Donation Program at the Forensic Anthropology Center at Texas State. The anatomical gifts of these individuals are essential to the continued development of forensic anthropology and taphonomy. To the Forensic Anthropology Center at Texas State, the Graduate College, the Grady Early Foundation, and the Freeman Center, many thanks for providing the financial and logistical support that allowed me to further my education and pursue this project.

Next I would like to thank the members of my thesis committee, who were instrumental to the success of this project. To Drs. Herrmann and Wescott, thank you both for your advice on methodology and statistics. Special thanks also to J.P. Fancher, whose astute observations provided the inspiration for this project, and who was always available with a word of encouragement or sage advice. To Dr. Michelle Hamilton, my committee chair and mentor, your support saw me through this program. Thank you for teaching me to maintain a healthy balance of skepticism, humility, and humor.

I would also like to thank my cohort. It has been a blessing and a pleasure to struggle and grow alongside you over the last two years. I feel honored to have gotten to know each of you, as professionals and friends, and I am so excited to see where all of you go from here. To Autumn and Kate, (royal) we did it! Thank you, thank you, thank you for your friendship.

Finally, I want to thank my family. To my significant other, Liam, I know the past two years have been a rollercoaster. Nevertheless, you have always been there for me when I needed you most, whether it was with a hug, a glass of wine, or an empty dishwasher. And to our four-legged girls, Lucy, Grace, and Ginger, thank you for being my comic relief, my alarm clock, and my best reason to close my laptop, leave my desk, and go for a walk.

TABLE OF CONTENTS

Page

LIST OF TABLES

Table **Page**

LIST OF FIGURES

Figure **Page**

LIST OF ABBREVIATIONS

Abbreviation	Description
ADD	accumulated degree days
ADS	accumulated decomposition score
BMI	body mass index
DIC	deviance information criterion
EDI	early decomposition indicator
FACTS	Forensic Anthropology Center at Texas State
FARF	Forensic Anthropology Research Facility
FPS	first protruding stain
N	normal (BMI category)
Ob	obese (BMI category)
Ov	overweight (BMI category)
PMI	postmortem interval
TBS	total body score
U	underweight (BMI category)
VOC	volatile organic compound

I. INTRODUCTION

Project Objectives and Significance

This study was conducted to document variability in the manifestation and timing of microbe-driven events in human decomposition, specifically: (1) bloating of remains, (2) purging of decomposition fluids, and (3) collapse or caving in of soft tissues. The occurrence of bloat, purge, and collapse are frequently referenced as being useful for estimation of the postmortem interval (PMI), or the time that has occurred between a decedent's death and the present (Galloway et al. 1989; Megyesi et al. 2005; Reed 1958; Rhine and Dawson 1998; Rodriguez and Bass 1983). In the forensic context, a PMI estimate may be used to narrow down lists of potential decedents, establish timelines of postmortem events, substantiate witness testimony, or in cases of violent death, corroborate or disprove the alibis of potential suspects. Consequently, it is important that possible variation in the early decomposition processes used in PMI estimates be addressed.

However, there are several potential problems with the way these events are currently defined and used in PMI estimation. Throughout the literature, bloat, purge, and collapse are typically presented as discrete traits (i.e., either present or absent) despite being part of the continuous process of human decomposition. Additionally, descriptions of these events are often generic, with little discussion on how to recognize their starting and ending points. This project attempts to refine our understanding of these early soft-tissue decomposition markers by dividing bloat, purge, and collapse into quasi-discrete, visually-observable indicators that attempt to account for observations that appear to straddle the lines between pre-bloat, bloat and purge, and post-bloat (i.e., collapse).

In previous studies, the general processes of bloat and purge have been used to define stages of human decomposition (Galloway et al. 1989; Rhine and Dawson 1998; Rodriguez and Bass 1983) and, from these stages, estimate PMI (Megyesi et al. 2005). My project examined the observed variance in the timing of specific indicators by modeling the probability that an indicator had occurred after a specified PMI, to determine whether the indicators provide the accuracy and precision needed for use in PMI estimations. The relationships revealed by these models may later be used to construct a new predictive model to estimate the PMI for cases discovered during early and mid-stage decomposition. Such a model would use the presence or absence of a suite of indicators to predict a PMI interval in which the combination of indicators was likely to have occurred. In short, this project addresses the following questions:

1. Are sequential, visually-observable indicators of early decomposition related to bloat, purge, and collapse available to characterize and refine PMI estimations?
2. Do intrinsic variables such as sex, body size, cause of death, or bodily trauma impact the timing of these early decomposition indicators (EDIs)?
3. Can the probability of these EDIs having occurred be modeled accurately given accumulated degree days and/or relevant intrinsic variables?

Bloat, Purge, Collapse, and Accumulated Degree Days

Bloat occurs when body cavities (e.g., digestive and respiratory tracts, circulatory system) fill with gases. These gases are generated by the metabolic processes of enteric microorganisms, which play a major role in the breakdown of bodily soft tissue after death. As these gases accumulate inside the body, gaseous pressure increases, causing the

soft tissues to swell and the body to inflate (Gill-King 1997; Hyde et al. 2015; Vass et al. 2002). Microbial breakdown simultaneously liquefies soft tissues, which are expelled from the body as the gaseous pressure increases. These liquids typically exit the body via natural orifices, such as the nostrils or mouth, or through areas where the integrity of overlying soft tissue has been reduced by traumatic injury or postmortem damage (Hyde et al. 2015; Vass et al. 2002). This process of liquid expulsion is known as purge. Collapse of the body occurs when the pressure exerted by accumulated gases is released, and air pressure is greater than gaseous pressure inside the body.

Bloat and purge are driven simultaneously by microbial metabolic activity and the two events are intimately related, as the physical buildup of gases produces the force that pushes liquefied tissue from the body (Hyde et al. 2015; Vass et al. 2002). These metabolic processes, mediated by microbial enzymes, are catalyzed by increases in temperature (Gill-King 1997; Hyde et al. 2015; Vass et al. 2002). Consequently, the timing of the two events is related to the ambient temperature in which the microbial communities exist. Like the trends observed in overall decomposition, it is assumed that the timing of bloat and purge is accelerated by increases and decelerated by decreases in ambient temperature (Mann et al. 1990). As bloat is accelerated or delayed, the timing of collapse would be expected to change accordingly.

With this expectation, it may be possible to predict the timing of these specific decomposition events using a variable that encompasses both temperature and time, accumulated degree days (ADD). Variation in climatic variables during periods of postmortem exposure make predicting postmortem interval using calendar days difficult, as these changes may accelerate or suppress the rate of decomposition processes. In

contrast, ADD incorporates what is generally accepted as the most significant variable – ambient temperature – into a predicted PMI (Campobasso et al. 2001; Mann et al. 1990; Rodriguez and Bass 1983). ADD treats temperature as a unit of energy that is available to power the metabolic and reproductive activities of necrophagous microorganisms and invertebrates (Vass et al. 1992). By estimating PMI in ADD, daily fluctuations in temperature at a death scene can be accounted for, increasing the precision and accuracy of PMI estimates. Since ADD was introduced into the field of forensic anthropology, numerous studies have demonstrated that using ADD instead of calendar days (e.g., bloat typically occurs between x and y ADD instead of x and y days) for PMI estimations significantly improves predictions (Marhoff et al. 2016; Megyesi et al. 2005; Myburgh et al. 2013).

Human Decomposition Stages

The process of decomposition has traditionally been subdivided into distinct stages, each characterized by major physical changes to the remains. One of the earliest schemas for mammalian decomposition was initially presented by Reed (1958) in a study of the insect colonization of dog carcasses. This system was adapted by Rodriguez and Bass (1983) for application to human remains and ultimately refined by other scholars including Galloway et al. (1989) and Rhine and Dawson (1998). Reed's (1958) stages included:

1. Fresh stage, characterized by condition of the carcass immediately after death
2. Bloated stage, characterized by inflation of the carcass due to accumulated gases
3. Decay stage, characterized by deflation and collapse of the carcass and moist decomposition

4. Dry stage, characterized by tissue loss, gradual desiccation of remains, and reduction of insect activity

Reed's (1958) decomposition stages were very broadly defined and only accounted for the decomposition of soft tissue, emphasizing periods of high insect activity, and indeed these stages are generally effective in studies of entomological succession, such as that completed by Rodriguez and Bass (1983). However, in more holistic studies of decomposition, researchers have sought to refine these stages.

Galloway et al. (1989) devised a five-stage system of human decomposition, where the first three stages roughly map on to Reed's (1958) four stage system. The fresh stage corresponds to the conditions of the remains immediately following death, prior to discoloration or insect activity. Early decomposition begins with the presence of tissue discoloration and skin slippage and proceeds through the completion of bloat. The third stage, advanced decomposition, begins with the collapse of the abdominal cavity and may include either moist decomposition, mummification, or both (Galloway et al. 1989). Advanced decomposition ends with skeletonization, which is characterized by the loss of soft tissue and substantial bone exposure, with or without retained grease (Galloway et al. 1989). As bones are exposed to the environment, they become subject to the final stage, extreme decomposition, which includes all processes that affect the decomposition of the skeletal material itself, including bone staining, sun bleaching, and weathering (Galloway et al. 1989).

Rhine and Dawson (1998) created another system of decomposition from casework conducted in the American Southwest, this time assigning each stage an ordinal score from 1 (completely fresh) to 15 (significant bone degradation and loss), assuming a

consistent progression through these stages across the casework. This study attempted to correlate these scores with known time since death, measured in weeks. While there was a general curvilinear relationship between decomposition stage and time since death, the authors discovered considerable variation in the stages achieved for cases recovered between one and three months after death (Rhine and Dawson 1998). Although the stages themselves were fairly predictable, the rate at which they were achieved was accelerated or slowed by case-specific variables, rendering them too imprecise to be used for accurate PMI estimations.

Taphonomic Agents and Human Decomposition Rate

As the study by Rhine and Dawson (1998) demonstrates, the rate of decomposition is not universal, making PMI estimation from stages of decomposition tricky. Variation in decomposition rate stems from the ecological role of decomposition as a process of nutrient recycling, characterized by the breakdown of organic tissues into their basic components, which can then be used by other living organisms (DeVault et al. 2003). Consequently, the process of decomposition is multivariate, influenced by both extrinsic (i.e., deriving from the environment and other organisms within it) and intrinsic (i.e., deriving from the remains themselves) variables.

In an early study of variation in human decomposition, based on observations of human cadavers placed at the Anthropology Research Facility at the University of Tennessee at Knoxville, Mann et al. (1990) proposed an initial ranking of several of these variables. Of the variables reviewed, three appeared to have the most significant impact on decomposition rate: (1) temperature, (2) insect access, and (3) burial (as opposed to exposed placement at the surface) or depth of burial (Mann et al. 1990). Other notable

variables discussed in this brief report include activity by animal scavengers, the presence of trauma or postmortem damage, and body size (Mann et al. 1990). Various cases from the study by Rhine and Dawson (1998) further supported the important roles of seasonal temperature, humidity, and carnivore access in shaping variation in the decomposition process.

Research has since been conducted on many of these variables in attempts to establish quantitative relationships between specific variables and the decomposition process, with the intent of constructing improved predictive models for estimating PMI. Many of these variables stem from changes in the environment in which remains are deposited, including climatic conditions and weather, which in turn affect the contributions of biological organisms.

Archer (2004b) looked at the influence of seasonal weather variables on the decomposition of neonatal pig carcasses at a field site in Canada, with five piglets placed in each season over the course of two years. The results of the study indicate that increased rainfall accelerated the rate of decomposition for neonate piglets, achieved through multiple possible mechanisms: chemical and mechanical degradation of soft tissue, leaching of body fluids, or maintenance of moisture in the soil and tissue which promoted the action of microorganisms and insects (Archer 2004b). Increased temperature in spring and summer months also contributed to increased rate of decomposition by promoting rapid maggot proliferation (Archer 2004b).

The results of Archer (2004b) supported relationships indicated in an entomological study by Lopes de Carvalho and Linhares (2001), which looked at seasonal changes in insect succession and decomposition in southeastern Brazil. The

results indicated that seasonal differences in temperature and rainfall significantly affected insect colonization of adult pig carcasses, with carcasses deposited during the summer – a warm and rainy season – decomposing at twice the rate of carcasses placed during other seasons (Lopes de Carvalho and Linhares 2001). While the authors found that the abundance of adult flies dwindled due to heavy rainfall during the summer, the abundance of larvae was much higher (Lopes de Carvalho and Linhares 2001).

Climatic variables such as temperature, humidity and rainfall influence the physical and chemical processes of tissue decomposition (Gill-King 1997). However, perhaps more importantly, these environmental variables mediate the role of biological organisms – including microorganisms, insects, and scavenging animals – that contribute to the breakdown of soft tissues. Microorganisms involved in decomposition derive from three sources: (1) enteric microfauna, or those originating from the dead organism's microbiome, (2) the soil or other substrates in contact with the decomposing remains, and (3) insects and animals that come into contact with the remains during decomposition (Hyde et al. 2015).

Initially, the microbial community associated with decomposing remains is dominated by families associated with the living microbiome, which are fairly unique from case to case (Hyde et al. 2015). As decomposition progresses, microorganisms from the environment (e.g., local soil, water, necrophagous insects, or scavenging animals) join the enteric microfauna. Consequently, the microbial communities of remains decomposing in the same environment will converge (Hyde et al. 2015). During decomposition, changes in the diversity of these communities and the abundance of different microbial taxa correspond to major taphonomic events such as the transition

from early to late decomposition (i.e., abdominal collapse), loss of wet biomass, and skeletonization (Hyde et al. 2015). Specifically, microbial communities are dominated by aerobic taxa during early decomposition, with a prominent shift toward anaerobic taxa as remains enter drier, more advanced decay (Cobaugh et al. 2015).

Microbial communities associated with decomposition are significantly influenced by seasonally-dependent climatic variables. Carter et al. (2015) compared the microbial communities present in control soils (i.e., those not associated with a grave) and post-rupture grave soils (i.e., grave soils following the completion of bloat and the collapse of the abdominal cavity) collected during summer and winter. The bacterial communities of control soils were significantly different from each other between the seasons, and post-rupture grave soils collected in both seasons were significantly different from their corresponding controls (Carter et al. 2015).

Winter post-rupture grave soil, although significantly different, was not as distinct from its control as the summer post-rupture grave soil. This finding suggests that shifts occurring in grave soil bacterial communities may be shaped by the proliferation of bacteria originating from the soil, not those originating from the remains (Carter et al. 2015). However, microorganisms associated with the microbiome have also been shown to remain in soil for several months after the completion of wet decomposition and the depletion of soft tissue resources, and thus their contributions to grave soil microbial communities cannot be completely disregarded (Cobaugh et al. 2015).

Microbial communities also serve to promote the recruitment of other biological organisms to a carcass. Carter et al. (2015) noted that bacterial communities facilitated eukaryotic (e.g., amoebae and fungi) proliferation in summer grave soil, as bacterial

metabolic processes created a favorable environment for eukaryotic growth by depleting soil moisture and increasing soil acidity. Microorganisms associated with decomposition also produce volatile organic compounds (VOCs), gases associated with quorum sensing signaling, a form of microbial communication (Tomberlin et al. 2012). Many VOCs are attractive to different insect species, including blow flies (*Lucilia sericata*), consequently recruiting insects to a carcass and promoting feeding and oviposition, thereby accelerating decomposition (Tomberlin et al. 2012). While VOCs are associated with putrid odors and may be detected by animal scavengers, the occurrence of animal scavenging of remains is moderated by many other toxic metabolic compounds produced by microorganisms (DeVault et al. 2003).

Although many species of insect may be associated with decomposing remains, there are two key orders of forensic significance: (1) Diptera (flies) and (2) Coleoptera (beetles) (Campobasso et al. 2001). If remains are accessible, Diptera species are among the first to colonize, capable of locating remains within minutes (Campobasso et al. 2001). Diptera may oviposit or lay eggs on the remains within a few hours. Preferential locations for oviposition include the mouth and nose, which are characterized by moisture and protective shade and provide hatched larvae, colloquially known as maggots, with rapid access to nutritious internal tissues (Campobasso et al. 2001). Extreme temperatures, below 12°C and above 30°C, inhibits oviposition and retards larval development (Campobasso et al. 2001).

As maggot activity is a key agent in soft tissue destruction, inhibition of maggot colonization or development can significantly alter the rate and trajectory of decomposition (Anderson and VanLaerhoven 1996). Pechal et al. (2014) compared the

decomposition of pig carcasses decomposing under natural conditions to those that were inaccessible to insects for the first five days after death. Pigs that were inaccessible to insects decomposed much more slowly, remaining bloated for two to three times as long as the control pigs (Pechal et al. 2014). Without maggot activity reducing the integrity of the overlying skin, the gases responsible for bloating remained trapped within the body cavity. Interestingly, once the pigs were made accessible, they attracted a different, less diverse community of invertebrate taxa than their control counterparts (Pechal et al. 2014).

Simmons et al. (2010a, 2010b) confirm that delayed or excluded insect access significantly slows the rate of decomposition, while demonstrating the dominant role that insect activity – specifically maggot activity – plays in soft tissue decomposition. The two articles provide evidence that the reason for insect exclusion is secondary to the exclusion itself, with decomposition occurring at a similar rate in remains discovered indoors, buried, or submerged, even when other variables are under experimental control (Simmons et al. 2010a; Simmons et al. 2010b). Furthermore, Simmons et al. (2010a) demonstrates that when insects are excluded, body size has no significant effect on decomposition rate.

When accessible to insects, Simmons et al. (2010a) found that smaller carcasses decomposed more quickly than larger carcasses, as maggot masses could colonize and consume a smaller carcass relatively quickly. Additional research (Archer 2004b; Sutherland et al. 2013) has come to similar conclusions. However, some researchers suggest that larger carcasses decompose more rapidly (Mann et al. 1990). Others suggest a conditional relationship between body size and decomposition rate dependent on

decomposition stage (Matuszewski et al. 2014; Spicka et al. 2011). A recent study of the impacts of body mass on decomposition rate of adult humans found no significant correlation between body mass and decomposition rate (Roberts et al. 2017).

The presence of penetrating trauma has anecdotally been thought to accelerate decomposition rate by creating new openings in the skin, thereby accelerating insect colonization of the internal body cavities (Campobasso et al. 2001). Cross and Simmons (2010) examined the relationship between gunshot trauma on the pattern and rate of decomposition of pig carcasses, while Bates and Wescott (2016) explored how autopsy incisions affected the decomposition of human cadavers. In a comparison of decomposition scores and body mass loss between control and experimental (shot) pigs, Cross and Simmons (2010) found no significant difference between the two groups in the decomposition rate from death to skeletonization. However, tissue loss was accelerated in the experimental group in early stages of decomposition, supporting a prominent role for trauma in promoting the proliferation of maggot masses (Cross and Simmons 2010).

Bates and Wescott (2016) also failed to find a significant a significant effect of penetrating trauma on the overall decomposition rate. Differences in the timing of individual decomposition stages were also insignificant, although the mean time required to reach each stage was slightly lower for the autopsied sample, indicating a slightly accelerated decomposition rate (Bates and Wescott 2016). This acceleration was attributed to increased internal temperatures noted in autopsied donations as well as increased insect access to internal tissues (Bates and Wescott 2016).

Postmortem freezing has also been implicated in changing the trajectory of decomposition. Decreasing temperature inhibits bacterial growth, and below 0°C, will

kill most enteric microorganisms. Consequently, microbial decomposition is suspended at freezing temperatures, and the decomposition of thawed remains is dominated by microorganisms originating from the external environment (Micozzi 1986; Micozzi 1997). The decomposition of previously frozen remains has thus has been described as occurring "from the outside in" (Micozzi 1997, 174), characterized by accelerated decomposition of external surfaces and decelerated decomposition of internal organs. Notably, previously frozen remains undergo a significantly reduced, often not visibly discernable, period of bloating and putrefaction (Micozzi 1997; Roberts and Dabbs 2015).

Total Body Score and Accumulated Degree Days

Breaking the process of decomposition into qualitative stages can help in estimating PMI. For example, if two bodies are found at the surface in the same location with one skeletonized and the other in the fresh stage of decomposition, it is often assumed that the skeletonized remains have been dead for longer than the fresh remains. This assumption, however, requires that neither set of remains were frozen, burned, dismembered, mummified, or otherwise manipulated in a way that impacts the decomposition rate. When remains are exposed to different taphonomic agents, the rate of decomposition can vary; consequently, the condition of human remains should be considered within the entire context of the death scene.

Relative PMIs of remains may occasionally be useful, as in the example described above. The absolute PMI, which estimates precisely when an individual died, is often the more pertinent forensic question. The broad, qualitative decomposition stages cannot make estimates of PMI with any precision. In an attempt to address this problem,

multiple decomposition scoring systems have been developed. These systems assign points to more specific characteristics of decomposing remains, which can then be used to calculate an absolute estimate of PMI.

Total body scoring (TBS), the first decomposition scoring system designed for forensic use on human remains, was developed from retrospective case photographs by Megyesi et al. (2005). The TBS method divided the body into three regions: (1) head and neck, (2) torso, and (3) appendages. Each of these bodily regions is given an independent score based on comparison of its physical characteristics and a series of specifically defined decomposition stages. The head and neck, for example, may receive a score of 1 point if it is fresh with no discoloration, a score of 7 if the decomposing tissue has begun caving in, or a score of 13 if it is completely skeletonized and dried (Megyesi et al. 2005). The TBS for the remains is the sum of the scores of each of the three bodily regions, ranging from a minimum of 3 (completely fresh) to a maximum of 35 (complete, dry skeletonization).

As previously mentioned, the rate of human decomposition is heavily influenced by ambient temperature. Consequently, temperature must be considered before a PMI estimate can be drawn from TBS. Megyesi et al. (2005) accomplished this through the use of ADD. When ambient temperature is higher over a given time period, more energy is available to necrophagous microorganisms and invertebrates, and their rate of activity and thus the rate of decomposition is expected to increase. This relationship allows observed, progressive changes in decomposition (via TBS) to be correlated with an expected ADD; Megyesi et al. (2005) used a standard least-squares linear regression of transformed TBS and ADD to define this relationship. The expected ADD can then be

converted to a PMI estimate in days using daily average temperatures from the environment where the remains were discovered (Megyesi et al. 2005).

Problems with the Total Body Score Approach

A study of interobserver error of the TBS method has demonstrated that the method is highly reliable, although concerns remain over its validity (Dabbs et al. 2016). Within the scoring system, many of the criteria are somewhat subjective. For example, in the head and neck, 7 points are assigned for "Caving in of the flesh and tissues of eyes and throat," while 8 points are assigned for "Moist decomposition with bone exposure less than half that of the area being scored" (Megyesi et al. 2005). However, couldn't one interpret the collapse of the face as being along the trajectory of moist decomposition? What criteria mark the transition between 7 and 8 points? The inclusion of color further complicates the equation, as it is highly variable between individuals. Megyesi et al. (2005) generally documents a trend from flesh-colored, to gray-green, to brown-black discoloration in the TBS criteria. What if, as the author has observed, the flesh takes on a yellow to orange hue? Overall, the method of Megyesi et al. (2005) leaves a lot of room for individual interpretation. Consequently, it is not a method that is well-suited for use by individuals with limited experience.

Gleiber et al. (2017) recently proposed a similar methodology using Accumulated Decomposition Score (ADS) instead of TBS, a new decomposition scoring system that follows the broad model introduced by Megyesi et al. (2005) but incorporates different criteria. ADS captures major, universal decomposition landmarks (e.g., marbling, skin slip, and bloat) while minimizing the noise introduced by individual variation. Like TBS, ADS scores individual body regions independently, but goes further to score upper limbs

separately from lower limbs, which often decompose at different rates. Given the high variation in color changes that occur during decomposition, ADS also removes color-specific criteria from consideration, instead scoring discoloration as either "present" or "absent." A high correlation between ADS and ADD was documented using an exponential regression, with ADD explaining over 80% of the variation in ADS (Gleiber et al. 2017).

Problems with Estimating ADD from TBS

Unfortunately, subsequent tests of the TBS and ADD estimation equation proposed by Megyesi et al. (2005) have identified a number of problems with the method as published. Suckling (2011) found that the ADD estimation method has high accuracy in predicting the ADD of remains with a TBS below 22 in south Central Texas, but very poor precision due to a high standard error; according to the Megyesi et al. (2005) formula, a fresh body (TBS 3) and a body in advanced decomposition (TBS 23) could have the same ADD within a 95% confidence interval. This could explain the general concordance with the Megyesi et al. (2005) method ADD estimations reported in a case study by Parks (2011), which included an analysis of a single cadaver in early stages of decomposition at the same facility. Suckling (2011) also noted the poor general performance (including accuracy and precision) of the Megyesi et al. (2005) method for cases in advanced stages of decomposition and skeletonization, finding that the method was biased toward overestimation of ADD for these cases.

Temperate climates are also subject to problems of PMI estimation using the method proposed by Megyesi et al. (2005). Parsons (2009) conducted a systematic study of the process of decomposition in central Montana and found that the Megyesi et al.

(2005) method produced underestimates of the PMI for early stages of decomposition, or low TBS. The author attributed these underestimates to decompositional stasis that accompanies environmental conditions of low temperature and humidity, prolonging the fresh stage of decomposition (Parsons 2009). Parsons (2009) also noted that similar underestimations may occur in mummified remains, which are also suspended in decompositional stasis. Like the Suckling (2011) study, Parsons (2009) also found that the high standard error of the original Megyesi et al. (2005) formula contributed to poor precision of PMI estimates.

Rather than testing the original Megyesi et al. (2005) formula, Myburgh et al. (2013) employed the methodology to construct a new ADD estimation formula specific to a temperate region of South Africa. Unfortunately, a validation study of their formula demonstrated that this region-specific formula had poor accuracy. The authors attribute the poor accuracy of their formula to high variation in the environmental characteristics that affected their sample, including pig carcasses deposited between August 2008 and February 2009 (Myburgh et al. 2013).

Both Parsons (2009) and Suckling (2011) found that the accuracy of the original Megyesi et al. (2005) ADD estimation method was high, but the high standard error in the formula renders the method imprecise, limiting its usefulness in a forensic context. These studies also demonstrated that although the original formula was developed from a national sample, it is not generalizable to remains placed in different climatic zones and microenvironments. In designing and testing a new regression formula for PMI estimation from TBS and ADD, Myburgh et al. (2013) further demonstrated that seasonal environmental differences can impede the accuracy of predictions, and suggest that

season-specific formulae be developed in temperate environments to account for changes in variables like solar radiation, precipitation, and seasonal changes in insect and vertebrate scavenger activity. Using ADS, Gleiber et al. (2017) constructed and tested season-specific regression equations and found that, generally, season-specific formulae were better predictors of ADD than the all-season formula.

Problems with Estimating PMI from ADD

Assuming ADD can be accurately and precisely estimated from TBS, converting ADD estimates to PMI estimates in forensic contexts can be challenging. Converting an ADD estimate to an estimated PMI requires knowledge of the daily average temperatures at the site where the body was found. In decomposition research, this data can be measured directly using a portable temperature data logger. However, in outdoor forensic cases, measured hourly temperatures are unavailable, and daily average temperatures must be retrospectively estimated from existing sources, often from weather stations located some distance away from the actual recovery site. The quality of the PMI estimate, therefore, hinges on the how accurately the selected temperature source data reflects the actual temperature at the site. Dabbs (2010) has demonstrated that, in the United States, indiscriminate utilization of weather data from the nearest meteorological station to a crime scene is inappropriate and can lead to error in PMI estimates.

To correct for differences between retrospective weather station data and actual site temperatures, forensic entomologists will often place a remote temperature logger at the site where a body is found for a brief correlation period. After this data is collected, temperature data recovered from the logger can be regressed against temperature data

measured by nearby weather stations, and the regression equation can be used to adjust retrospective temperature data from the weather station (Archer 2004a).

Archer (2004a) was the first to assess this correlation method of data adjustment. He found that while the accuracy of temperature data was generally improved by the correlation method, the accuracy of corrected data declined as temperature differences between the period used to construct the model and the retrospective period (i.e., the period when the body was in place) increased (Archer 2004a). A follow-up study by Johnson et al. (2012) found that temperature differences greater than 5°C failed to improve accuracy of corrected weather data. Consequently, it is important that if a corrective regression is constructed, the data used is collected during similar weather conditions and seasons that the body has been in place.

The correlation method employed by forensic entomologists attempts to correct temperature data taken over relatively short periods of time, as the goal is to estimate the time required for necrophagous insect development to a specific life stage. Given the nature of the discipline, forensic anthropologists are often called to the scene for skeletonized cases that may have PMIs of months to years. Unfortunately, as a recent study by Dabbs (2015) has demonstrated, the correlation method used by forensic entomologists does little to improve the accuracy of retrospective temperature data over extended timespans. Instead, Dabbs (2015) recommends that practitioners use uncorrected data while taking into consideration the known level of error, rather than increase the likelihood of introducing error through attempted adjustments.

II. METHODS

Research Facility

Data was collected from the Forensic Anthropology Research Facility (FARF) at Texas State University, located on Freeman Ranch in San Marcos, Texas. Freeman Ranch is a working ranch and educational facility located just northwest of San Marcos and is situated within the Edwards Plateau (Barnes et al. 2000). The soils of the ranch are shallow and rich with clay, overlying large limestone deposits (Barnes et al. 2000). As of 2000, vegetation characteristic of grassland environments covers approximately half of the terrain of Freeman Ranch, consistent with a long-term trend of encroaching woodland species following European settlement of the region in the 1800s (Barnes et al. 2000).

The climate at Freeman Ranch is sub-tropical. Summer highs often surpass 90°F (>32°C) while winter lows rarely sink below 40°F (~4°C), and the area has an average annual relative humidity of approximately 67% (Dixon 2000). Freeman Ranch receives approximately 34 inches of rain in an average year, with most falling during the late summer and early fall, a period which coincides with the Atlantic hurricane season (Dixon 2000). Given the general scarcity of rainfall, the area is vulnerable to drought, although severe flooding also occurs periodically. Freeman Ranch is home to a diverse biological community, including both livestock and wild vertebrate species (Baccus et al. 2000). Most of the mammalian species – such as raccoons (*Procyon lotor*) and opossum (*Didelphis virginiana*) are facultative scavengers that will consume carrion, or dead animal tissue, when it is available (Sincerbox and DiGangi 2018). Obligate scavengers, including American black vultures (*Coragyps atratus*) and turkey vultures (*Cathartes*

aura), are also frequent visitors to FARF and have been the subjects of multiple research projects at the facility (Klein 2013; Reeves 2009; Spradley et al. 2012).

Sample

Human cadavers used in this study were obtained from the Forensic Anthropology Center at Texas State's (FACTS) Willed Body Donation Program. Donations are acquired by FACTS with consent from pre-registered donors or from a donor's legal next-of-kin, with donations accompanied by a survey including demographic information and summarized dental and medical histories (Forensic Anthropology Center at Texas State 2016). FACTS does not accept embalmed donations, those weighing over 500 pounds, or those with communicable diseases that can survive in or on a host for prolonged periods following death, including HIV, Hepatitis B, and Hepatitis C (Forensic Anthropology Center at Texas State 2016).

Data were collected *in situ* for 11 donations during the summer of 2017. A summary of the demographic information of this sample is presented in Table 1. For *in situ* data, this project only used donations that were in the fresh stage of decomposition upon arrival at the facility. Donations displaying any signs of early decomposition upon their arrival at the facility, such as marbling, skin slip, fluid-filled blisters, or discoloration (other than lividity) were not used. Autopsied donations, donations with significant trauma, and donations that were known to have been frozen prior to or during intake at FACTS were also excluded from this study. Although autopsied donations are reported to experience bloat (Bates and Wescott 2016; Cross and Simmons 2010), the objective of this project was to characterize bloat and purge under natural and non-traumatic circumstances, and it was anticipated that the presence of autopsy incisions or

major trauma could affect the degree of bloat observed or the pathways of purging fluids. Frozen donations were excluded due to the demonstrated effects of freezing on decomposition, which kills many of the enteric microorganisms which cause abdominal bloating (Micozzi 1997; Roberts and Dabbs 2015). Individuals with preexisting medical conditions that could impact their enteric microbial community, including infection and cancer, were noted. Individuals were considered to have cancer if their cause of death was attributed to cancer or complications of cancer. Individuals were considered to have an infection if their reported causes of death included a disease caused by microorganisms, or as a complication of such a disease. In this study, the two individuals considered to have had an infection had causes of death attributed to complications of pneumonia.

Table 1. Donations Used for *in situ* Data Collection

Donation Number	Sex	Age at Death	Ancestry	Weight (lbs)	Height (in)	BMI	Placement Date (M/D/Yr)
D30-2017	F	74	White	72	61.81	13.25	5/25/2017
D31-2017	M	58	White	87	65.74	14.15	5/26/2017
D37-2017	M	84	White	176	70.08	25.19	6/23/2017
D38-2017	M	88	White	161	66.14	25.87	6/30/2017
D40-2017	M	77	White	168	68.11	25.46	7/19/2017
D42-2017	M	55	White	128	70.08	18.32	7/21/2017
D46-2017	F	83	White	152	59.84	29.84	8/8/2017
D50-2017	M	97	White	118	65.35	19.42	8/23/2017
D51-2017	M	72	White	120	66.93	18.83	8/31/2017
D52-2017	M	94	White	102	68.11	15.46	9/1/2017
D55-2017	M	61	Black	489	67.32	75.85	9/7/2017

After visual indicators of bloat, purge, and collapse were identified, retrospective data were collected on a sample of 19 donations placed at FARF during previous summers (i.e., May – early September placement dates), which were photographed and documented as part of the facility's long-term longitudinal decomposition study. The

demographic information for the retrospective sample is presented in Table 2. As with the *in situ* data, only donations that were unautopsied, had minimal trauma, and were never frozen were considered for inclusion in the sample and cause of death was noted.

Table 2. Donations Used for Retrospective Data Collection

Donation Number	Sex	Age	Ancestry	Wt (lbs)	Ht (in)	BMI	Placement (M/D/Yr)
D15-2012	M	62	White	150	71.3	20.77	05/08/2012
D23-2012	M	56	White	220	71.3	30.46	06/19/2012
D24-2012	F	83	White	172	59.7	34.07	06/22/2012
D23-2013	M	63	White	150	68.9	22.21	05/06/2013
D44-2014	M	73	White	122	65.9	19.72	09/01/2014
D23-2015	M	69	White	170	67.7	26.06	06/08/2015
D25-2015	F	68	White	76	60.6	14.53	06/08/2015
D30-2015	M	86	White	156	70.5	22.08	06/08/2015
D35-2015	F	69	White	158	64.4	26.81	07/02/2015
D40-2015	M	83	White	128	65.0	21.32	07/29/2015
D43-2015	F	97	White	118	60.8	22.42	08/12/2015
D20-2016	M	78	White	140	67.1	21.84	07/05/2016
D22-2016	F	68	Black	163	62.2	29.61	06/10/2016
D39-2016	F	63	White	110	62.2	19.98	08/23/2016
D33-2017	F	64	White	109	63.0	19.31	06/20/2017
D34-2017	M	58	White	225	64.8	37.71	06/14/2017
D45-2017	F	83	Hispanic	101	60.2	19.57	07/31/2017
D53-2017	F	56	White	148	60.0	28.86	09/04/2017
D54-2017	M	69	White	120	71.3	16.61	09/06/2017

Data Collection

In situ Data Collection

The observation period began on May 25th, 2017 and continued through September 20th, 2017. Upon intake of the donor's body at the facility, cadaver weight and cadaveric stature were measured, in pounds and centimeters, respectively. These stature measurements were converted and rounded to the nearest inch to calculate body mass index (BMI). For several donations, an accurate cadaveric stature could not be taken because the bodies were in flexed rigor mortis upon arriving at the facility and could not

be repositioned. An estimated living stature, collected as part of an entry questionnaire to the Willed Body Donation Program, was used to calculate BMI in these cases. BMI was calculated for each donation using the formula recommended by the United States Center for Disease Control and Prevention (CDC) Division of Nutrition Physical Activity and Obesity (2014):

$$BMI = \left(\frac{weight\ (lbs)}{(height\ (in))^2}\right) x\ 703$$

Donations were then assigned to BMI categories using the classes recommended by the CDC Division of Nutrition Physical Activity and Obesity (2016) for adult Americans, presented in Table 3.

Table 3. BMI Categories for Adult Americans

Category	Abbreviation	BMI Range
Underweight	U	< 18.5
Normal	N	18.5 – 24.9
Overweight	Ov	25 – 30
Obese	Ob	> 30

All donations were placed on the surface in a supine position, with the exception the flexed donations, which were instead placed on their side. Flexible 60" fiberglass measuring tapes were placed underneath the abdomen of each donation, at the level of the navel. In later trials, beginning with the 7th donation (D46-2017), measuring tapes were also placed under the chest and neck to document differences in the timing and degree of bloat in different regions of the torso. Unfortunately, tapes could not be placed under the last *in situ* donation due to insufficient length of the tapes for circumferential measurements of the abdomen and chest.

Observations were made daily, beginning on the day of placement at the facility and continuing until abdominal collapse, or the caving in of the abdominal cavity, was

observed. Photographs were taken daily to allow for retrospective review of decomposition criteria, including an overall view of the donation as well as close-range anterior and lateral views of the head and torso. Measurements of abdominal circumference, as well as measurements of the circumferences of the chest and neck in the later trials, were recorded to the nearest tenth of a centimeter. To promote consistency of measurement locations through time, quasi-anatomical landmarks were used to align tapes during measurement. The navel was used as the landmark for the abdominal circumference. Chest circumference was taken inferior to the breast tissue. The measurements of the neck were taken at the base of the neck, below the thyroid cartilage.

Visual observations of bloat, locations and consistency of purge, and soil stain formation were recorded. Bloat observations recorded include protrusion of the tongue, swelling of the face and neck, visible abdominal distention, swelling of the scrotum (in males only), abdominal wrinkling, and abdominal collapse. Because many of these traits were subjective due to variation in their expression, specific definitions for EDIs that could be identified *in situ* and in photographs were developed. After definitions had been refined in late July, photographs and notes taken *in situ* were reviewed and revised as necessary to ensure consistency in the scoring protocol across the sample. The revised definitions for selected indicators – purge, facial bloat, abdominal distention, facial collapse, abdominal wrinkling, abdominal collapse, first protruding soil stain, and stain outline – are presented later in this chapter.

Retrospective Data Collection

Retrospective data were obtained from photographs taken as part of the multi-year longitudinal decomposition study at FARF. Donations were excluded if height or weight

data was missing from the intake report. Although these donations were included in the retrospective study, it was noted if donations may have been frozen for significant periods of time before placement at the facility, or if antemortem health or cause of death was likely to have influenced enteric microbial community compositions (e.g., cancer chemotherapy, bacterial infection).

Temperature Data Sources

For both retrospective and *in situ* samples, temperature data was collected primarily from a weather station located on Freeman Ranch. This station reports a temperature measurement (in Celsius) every 30 minutes. High and low temperature measurements for each 24-hour period were identified for use in calculating the daily average temperature. Where data from the on-site data logger was missing due to equipment malfunction (a period in late May and early June 2017), temperature data was collected from the San Marcos Municipal Airport (Station KHYI), publicly available from wunderground.com. KHYI data was converted from Fahrenheit to Celsius for calculations of daily average temperature. To ensure applicability of the KHYI data, the mean daily average temperatures for two weeks prior to the malfunction were statistically compared between the two sites (i.e., the Freeman Ranch data logger and the San Marcos Municipal Airport weather station) using a standard t-test. The test revealed no significant differences.

Accumulated Degree Day Calculation

For both samples, ADD was calculated for the period between placement of the donation at FARF and every observation. Mean daily temperatures were calculated using the formula below (McMaster and Wilhelm 1997). A base temperature of 4°C was used,

corresponding to the temperature at which microbial activity significantly slows (Micozzi 1997).

$$T_i = \left[\frac{(T_{max} + T_{min})}{2}\right] - T_{base}$$

Mean daily temperatures were summed to calculate the ADD required to achieve an indicator. The range of daily temperatures summed was inclusive, including the mean daily temperatures on all days since placement, including the date the observation was made. On the date of placement, an ADD of 0 was used, as observations were generally made at the time of placement before prolonged exposure to ambient temperatures at FARF.

Definitions of Early Decomposition Indicators (EDIs)

Eight EDIs were identified throughout the course of this research: facial bloat, abdominal distention, purge, first protruding soil stain, soil stain outline, facial collapse, abdominal wrinkle, and abdominal collapse.

Bloat

As previously discussed, bloat can be defined as the swelling of tissues due to accumulated gases produced by microbial decomposition. In this study, bloat in the facial tissues typically preceded bloat in the torso. Swelling of the face was identified by ballooning of the cheeks and tautness of the facial tissues, while swelling of the neck was identified by reduced definition of the jaw (Figure 1). Abdominal distention was visually identified by the tautness of overlying tissue, by the reduction of natural contours of the hips and waist, and the reduced definition of the rib cage; generally, the torso became more cylindrical as the abdomen inflated (Figure 2).

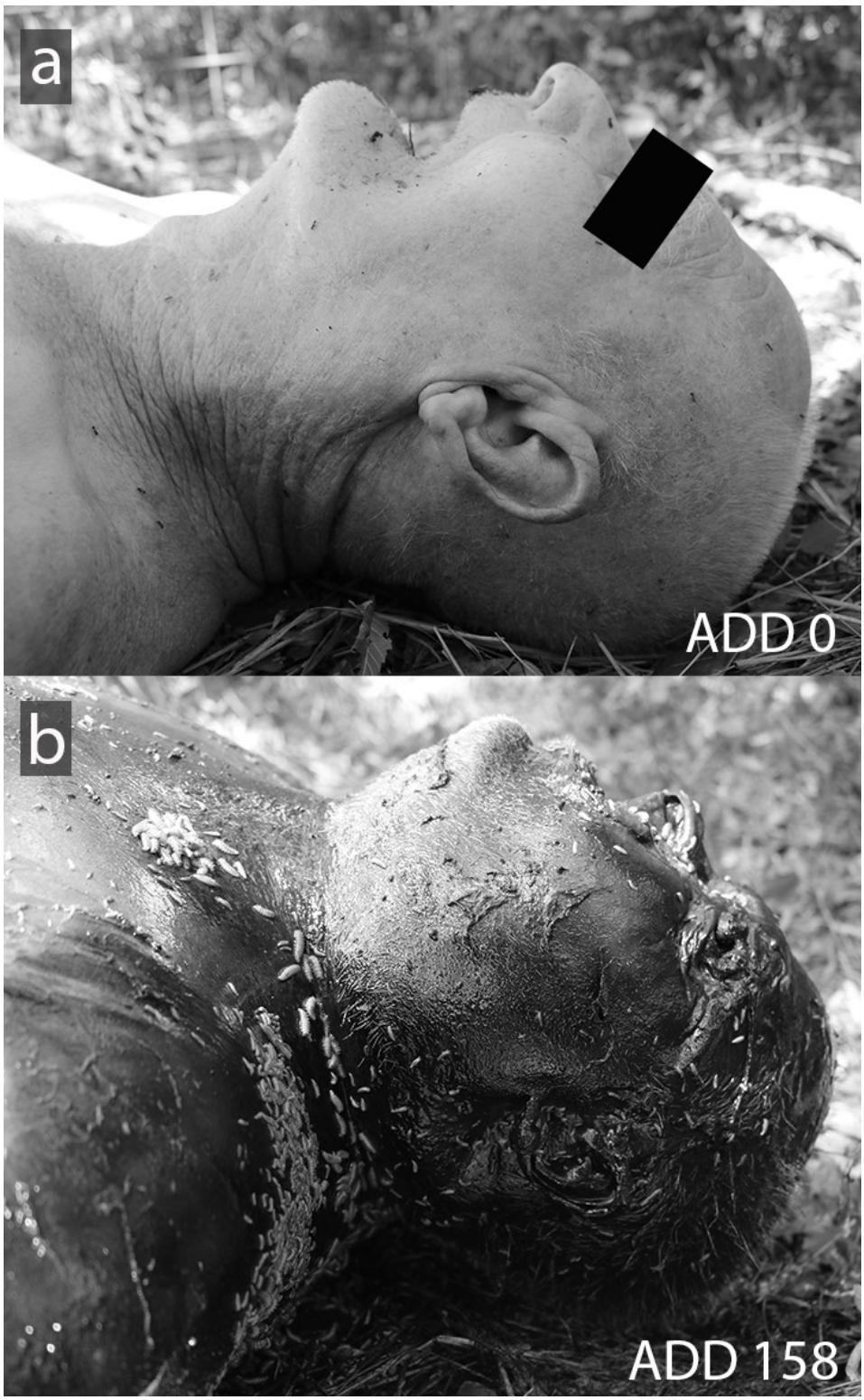

Figure 1. Facial Bloat. (a) Face and neck at time of placement (ADD 0) and (b) at 6 days (ADD 158). Note reduced definition of the jaw, indicating active bloating of the neck.

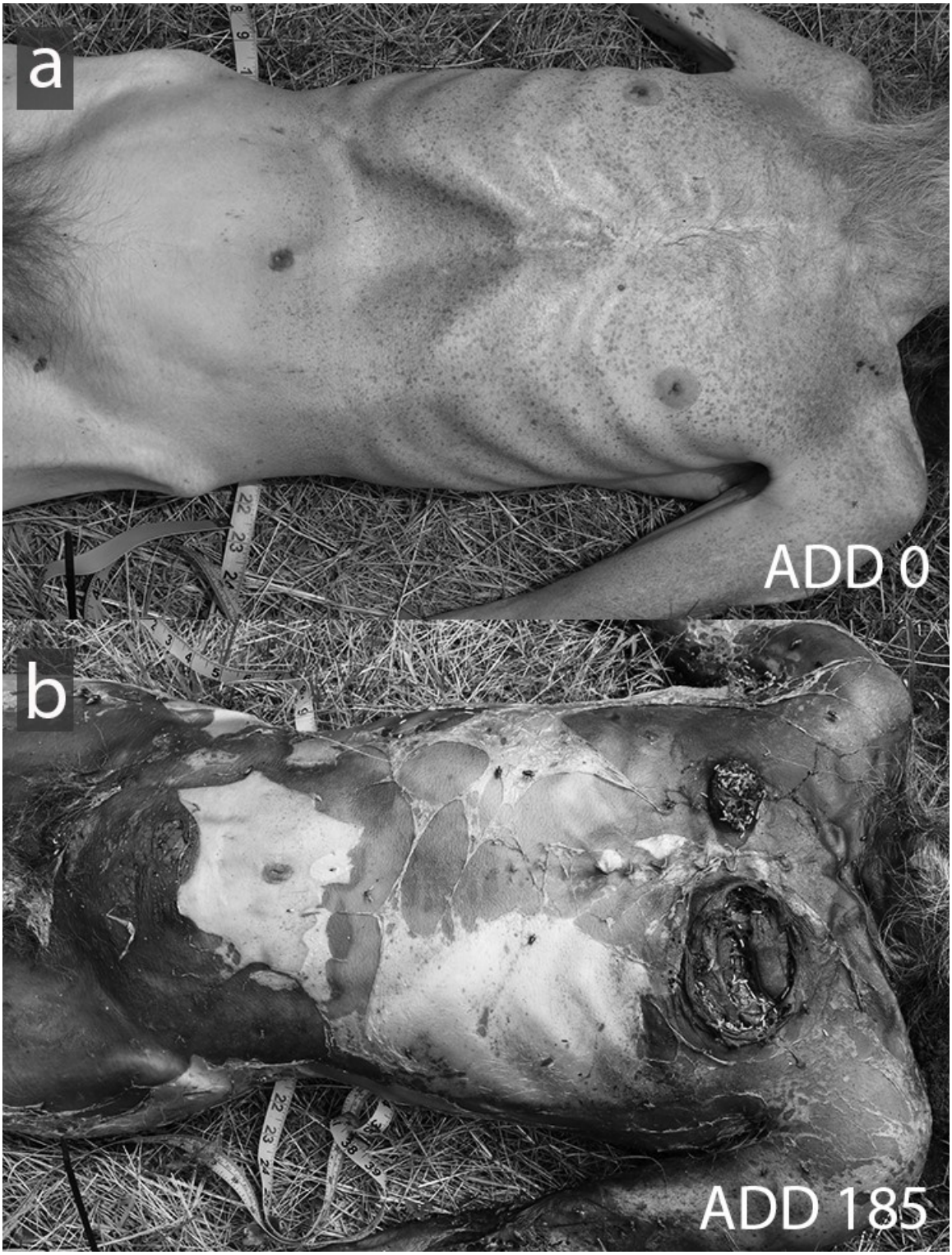

Figure 2. Abdominal Distention. (a) Torso at placement (ADD 0) and (b) at 7 days (ADD 185). Note swollen waist and reduced definition of rib cage, indicating active bloating of the torso.

Purge

Purge can be defined as the expulsion of decomposition fluids and liquefied tissues due to internal pressure, produced by the accumulation of gases inside the body cavities. Direct observation of active purge was rare. Although fluids frequently pooled in the mouth and nostrils of donations, it often could not be distinguished from fluid pooled due to previous rainfall or condensation. In some rare cases, bubbling was observed in these fluids, indicating that gas was escaping from the remains (Figure 3). Occasionally, fluid or liquefied tissue could be observed seeping directly from natural orifices or other openings. The consistency of purging substances varied considerably between individuals, as well as between different observations of the same individual throughout decomposition, including thin or viscous fluids, dark sludgy solids, and pale yellow-brown foam.

Figure 3. Active Purge. A direct observation of purge on day 4 (ADD 113). Note bubbles accumulated in the mouth.

Most often, active purge was identified by the presence of fluid pooled under or immediately adjacent to the body (Figures 4 and 5). This generally appeared under the head and neck before appearing under the torso and groin. Consequently, the presence of soil stains were often referred to in the absence of direct observation of purge. The first protruding soil stain, when the stain extends outside areas in direct contact with the body, was documented as a proxy for purge. Generally, this occurred first under the head and neck (Figure 4). Additionally, the appearance of a soil stain outline was documented (Figure 5). An outline was considered complete if the stain radiated away from the head and torso, outside of areas of direct contact between the body and ground, and staining was visible under the appendages.

Figure 4. First Protruding Stain. First protruding stain (FPS) adjacent to right neck and arm on day 4 (ADD 133), noted with white arrow. FPS was often difficult to observe from photographs due to the presence of shadows.

Figure 5. Soil Stain Outline. Soil stain outline on day 7 (ADD 188).

Collapse

Collapse occurs when the remains deflate, as gaseous pressure inside the body cavities decrease and the overlying epidermal tissue succumbs to gravity. Facial collapse usually preceded abdominal collapse (Figure 6). Cheeks appeared sunken, and features of the facial skeleton became more well defined. The epidermis often appeared very thin, and coloring of the facial tissue was often (but not always) dark brown to black.

Early deflation was evidenced by wrinkling of the epidermal tissue over the abdomen and appeared to be more common in individuals with higher BMIs (Figure 7). Wrinkles of interest appeared below the inferior border of the rib cage, but above the anterior margin of the pelvic girdle. Wrinkling in the neck, upper chest, and thighs appeared more inconsistently. Abdominal wrinkling was followed by full collapse of overlying tissues into the abdominal cavity, identified by a bowl-like depression in the soft tissues between the rib cage and the pelvis (Figure 8a). Occasionally, abdominal collapse manifested as a T-shaped indent in the abdomen (Figure 8b).

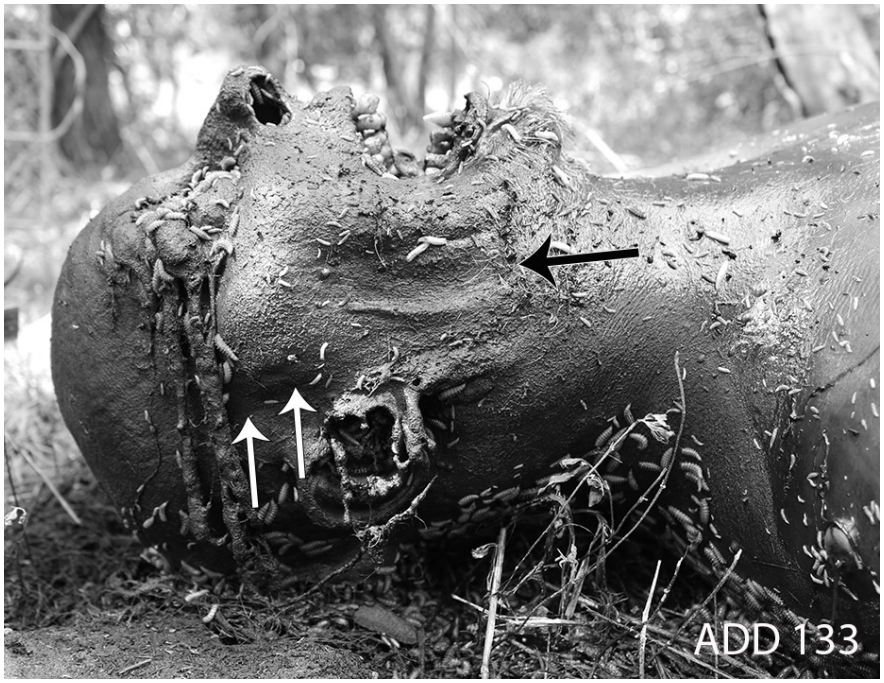

Figure 6. Facial Collapse. Facial collapse at 4 days (ADD 133). Note sunken cheeks (black arrow) and increasing definition of the underlying skeletal structure, here the zygomatic (white arrows).

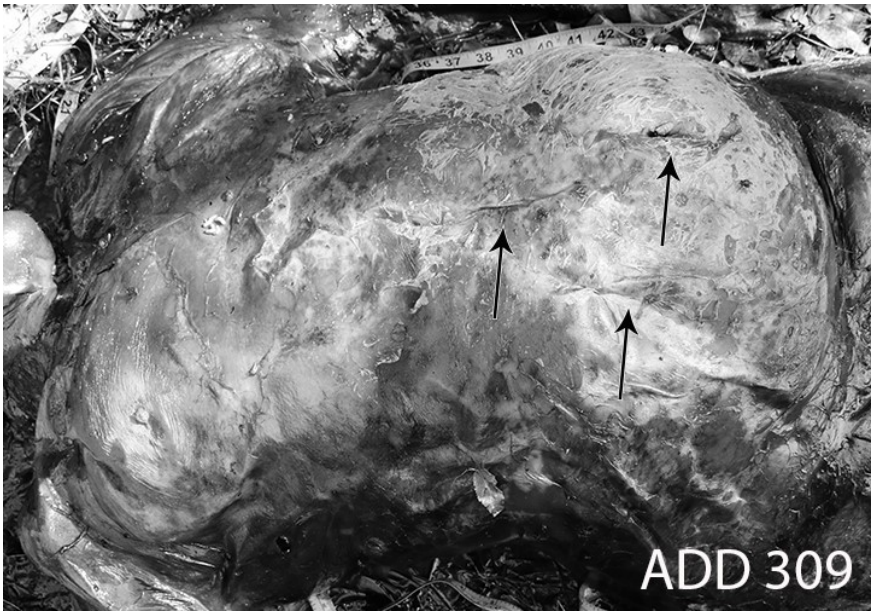

Figure 7. Abdominal Wrinkle. Abdominal wrinkling at 11 days (309 ADD). Several deep wrinkles in the region of interest, the abdomen, are indicated with black arrows.

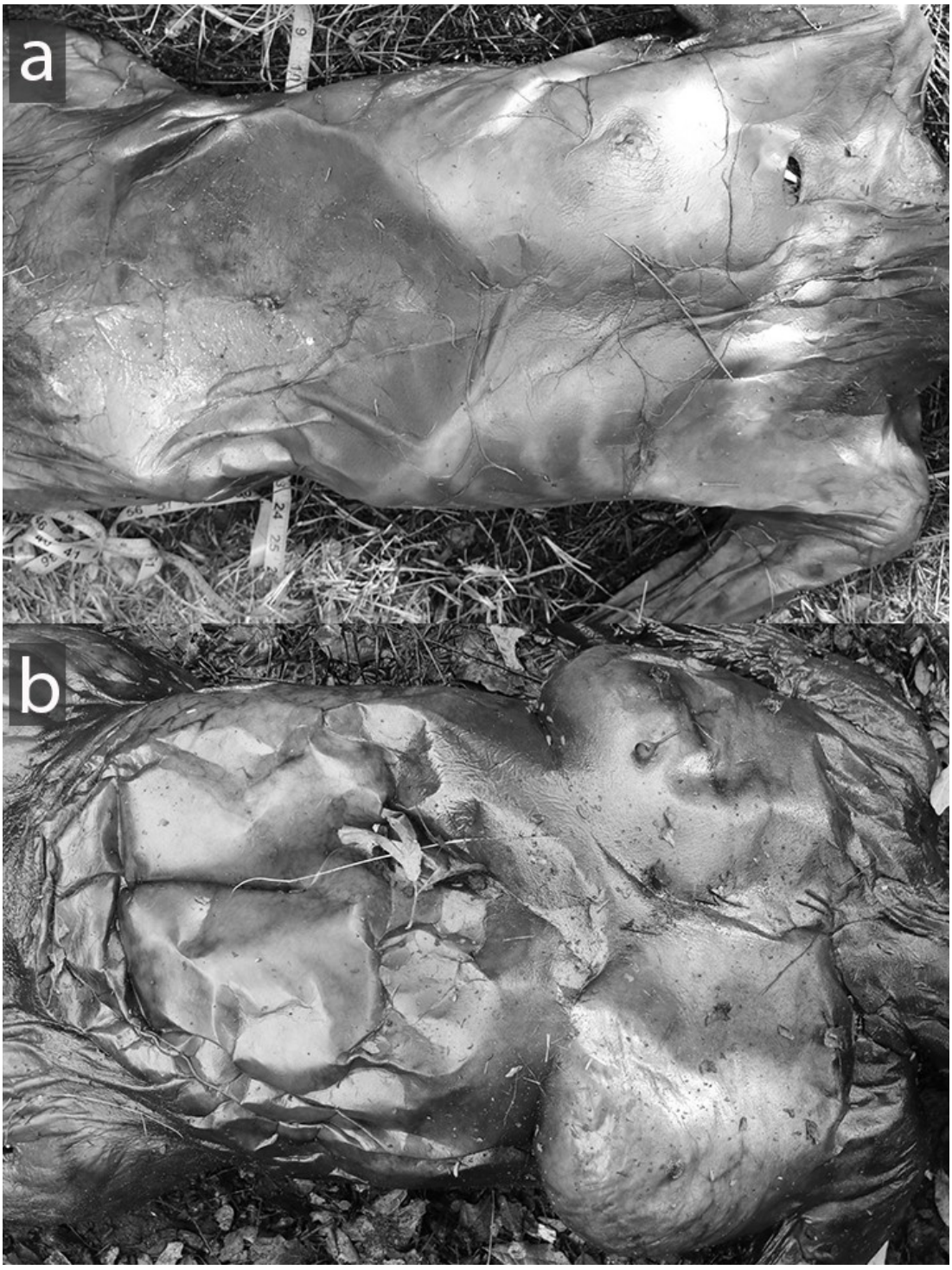

Figure 8. Abdominal Collapse. Abdominal collapse manifested as (a) a bowl-shaped depression or (b) heavy wrinkling of tissue overlying the abdominal cavity, often with a defined T- or H-shaped indent.

Data Analysis

ADD was calculated for the date that each of the eight EDIs was first observed in both *in situ* and retrospective donations, and the sample divided into the following groups for comparison:

1. Male / female
2. BMI classes (Underweight, Normal, Overweight, and Obese)
3. Cancer / no cancer
4. Trauma / no trauma
5. Possible infection / no infection

For each EDI, descriptive statistics were generated, including the mean and standard deviation of ADD to first appearance in all groups. Bar charts and scatterplots were constructed for exploratory analysis of possible influences of the intrinsic variables on the ADD to first appearance of EDIs. These figures are available in Appendix A. The distribution of the ADD data for the date of first appearance for each indicator was analyzed using the Shapiro-Wilks test. For indicators with a normal distribution, Bartlett's test was used to test the homogeneity of variances or homoscedasticity of the data between each group. For indicators with normally distributed data with equal variance, a t-test or one-way ANOVA (BMI class, only) was used to test for differences in the mean timing of indicator appearance between the groups. For indicators with non-normally distributed data or unequal variances, the more conservative nonparametric Mann-Whitney U-test or Kruskal-Wallis test (BMI class, only) was used to compare means. All statistical analyses were conducted in R-studio.

To further evaluate the influences of sex, BMI, cancer, possible infection, and trauma on timing of decomposition indicators, mixed effects models were used. Mixed effects models are also known as multilevel or hierarchical models. In contrast to classical regression models, mixed effects models accommodate the modeling of variation between groups within a dataset by allowing the coefficients and/or intercepts within the model to vary by group (Gelman and Hill 2007). They include both fixed and random effects. The coefficients of random effects vary by group and are produced as an outcome of the model, while the coefficients of fixed effects do not change from one group to the next (Gelman and Hill 2007). For this study, mixed effects models were selected because they can be designed to accommodate repeated observations on the same subjects by including subjects (i.e., donations) as random effects. Other benefits of mixed effects models include higher capacity for estimation from modest sample sizes and accommodation of unequal groups sizes or missing data (Gelman and Hill 2007).

The raw data was first subset into eight model datasets, one for each indicator. Within each model dataset, any observations coded as unobservable ("NA") for the trait of interest were removed. In addition, donations were removed from a model dataset if the collected data did not include observations of both indicator presence and absence. Three donations were removed from all models. D51-2017 bloated and purged on a trajectory that was fairly consistent with other donations considered in this study, but collapse indicators (abdominal wrinkle, abdominal collapse) were extremely delayed. This delay occurred only after evidence of scavenging of the donation's maggot masses was observed, including soil disturbance along the right side of the torso. This

scavenging event produced a marked disruption in maggot activity, which has previously been shown to delay later decomposition events (Pechal et al. 2014).

D46-2017 also demonstrated delayed decomposition patterns relative to other donations in this study and was associated with a neighboring donation that was subject to substantial scavenging. Although little scavenging was noted in D46-2017, it's possible that the presence of an active scavenger nearby disrupted normal insect activity. Because the impact of animal scavenging and insect activity was not in the scope of this project and therefore not evaluated in this study, D51-2017 and D46-2017 were removed from model construction datasets as outliers to improve model performance. D55-2017 was also removed from the model datasets due to their extreme BMI of 75.85, which skewed the mean and prevented appropriate scaling of the variable.

To ease model convergence, the data in each model dataset were truncated to encompass the minimum ADD when an indicator first appeared and the maximum ADD in which an indicator was still absent. Continuous variables included in each model (i.e., ADD and BMI) were scaled and centered for each model dataset by subtracting the mean value of the variable from the observed value, and dividing by the standard deviation of the variable in the dataset. A table of variable scaling formulae is available in Appendix B (Figure B1). Models for each indicator were then constructed and evaluated using the glmer function of the R package lme4 (Bates et al. 2015). The distribution of the model was set to binomial and default parameters for the glmer function were used with the exception of the nAGQ argument, which specifies the number of nodes used in the adaptive Gauss-Hermite quadrature that approximates the log-likelihood of the model (Bates et al. 2015). The default for the nAGQ argument is 1, corresponding to the

Laplace approximation. The nAGQ for these models was increased to 2 to induce model convergence but had the added benefit of improving the accuracy of the log-likelihood calculations (Bates et al. 2015).

The results of the exploratory analysis and comparison of group means were used to inform variables incorporated into model construction. Variables were retained in the model if they improved the model fit, indicated by reduced group-level variance (variance between random effects) and a decrease in deviance information criterion (DIC), which is a measure of fit similar to the Akaike information criterion that is appropriate for the structure of multilevel models (Gelman and Hill 2007). These measures were obtained using the display function in the R package arm (Gelman and Su 2016). A complete table of specifications for each model included in this thesis is available in Appendix B (Figure B2).

After mixed effects models for each indicator were constructed, predictive probability curves were produced for each model. For models incorporating BMI as a fixed effect, curves were produced for three different BMIs that encompassed a range of BMI classes: 15, 20, and 25. Models were tested using subsets of 30 observations from the original model datasets. Scaled ADD of each observation in the test sets were plugged into the model formula to calculate the probability that the indicator in question had occurred. Probabilities greater than 50% were considered present, while probabilities lower than 50% were considered absent. These predicted observations were compared to the actual observations, and the total proportion of matches and the rate of type I and type II errors were calculated. Observations in the test set were selected using a random number generator to select rows in the data frame, without replacement.

III. RESULTS

A summary of the ADD to the first observation of indicators for the entire sample (including the *in situ* and retrospective observations) is given in Table 4, including the minimum and maximum ADD observed as well as the mean and the standard deviation. The boxplot of this data (Figure 9) demonstrates the general sequentiality of indicator appearance from earliest (Facial Bloat & Purge) to latest (Abdominal Collapse).

Table 4. Descriptive Statistics for ADD to First Observation of EDIs

Indicator	Min. ADD	Max. ADD	Mean ADD	SD
Facial Bloat	47.04	175.92	91.60	32.25
Purge	44.43	175.92	94.95	39.38
Abdominal Distention	66.63	228.95	111.02	40.54
First Protruding Stain	94.35	228.95	138.66	32.57
Facial Collapse	101.92	237.66	153.72	32.76
Abdominal Wrinkle	121.30	309.05	179.88	53.85
Stain Outline	121.30	366.51	191.70	65.61
Abdominal Collapse	115.08	433.61	219.78	76.73

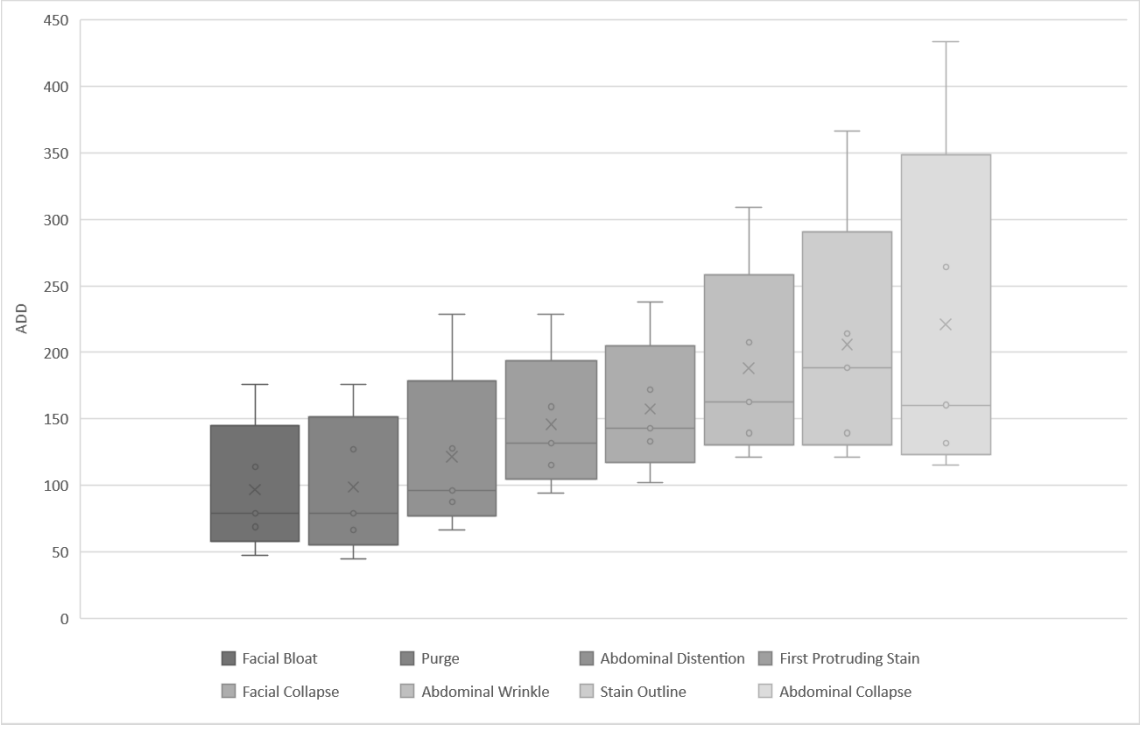

Figure 9. Box Plot of ADD at First Observation of EDIs.

Purge

Exploratory data visualization (see Appendix A, Figure A1) demonstrate a slight negative relationship between BMI and timing of first observed purge. Generally, individuals with higher BMIs appear to purge earlier than individuals with lower BMIs. Additionally, individuals with major abdominal trauma appeared to purge earlier than individuals without trauma (see Appendix A, Figure A11). There was no apparent difference between the timing of purge in individuals with and without cancer (see Appendix A, Figure A9), and the effect of infection could not be reliably explored due to the small number of individuals with infection (n=1) in the sample.

Table 5. Comparison of Mean ADD to First Observed Purge

Grouping	Group	n	Mean ADD	Test Used	Test Statistic	p-value
Sex	Male	12	95.92	Parametric	1.287	0.215
	Female	7	77.66			
BMI Class	Underweight	5	104.04	Parametric	0.650	0.595
	Normal	6	93.31			
	Overweight	6	77.73			
	Obese	2	74.14			
Cancer	Cancer-Free	13	91.99	Parametric	-0.172	0.867
	Cancer	5	89.23			
Trauma	No Trauma	16	92.07	Parametric	-1.669	0.119
	Trauma	3	73.87			

To explore the significance of these relationships, the means of each group were statistically compared (Table 5). The data was determined to have a normal distribution, and the variances in each group were homogeneous. Sex, cancer, and trauma groups were compared using Welch's t-tests, while BMI classes were compared using one-way ANOVA. Individuals with and without infection could not be reliably compared, as only

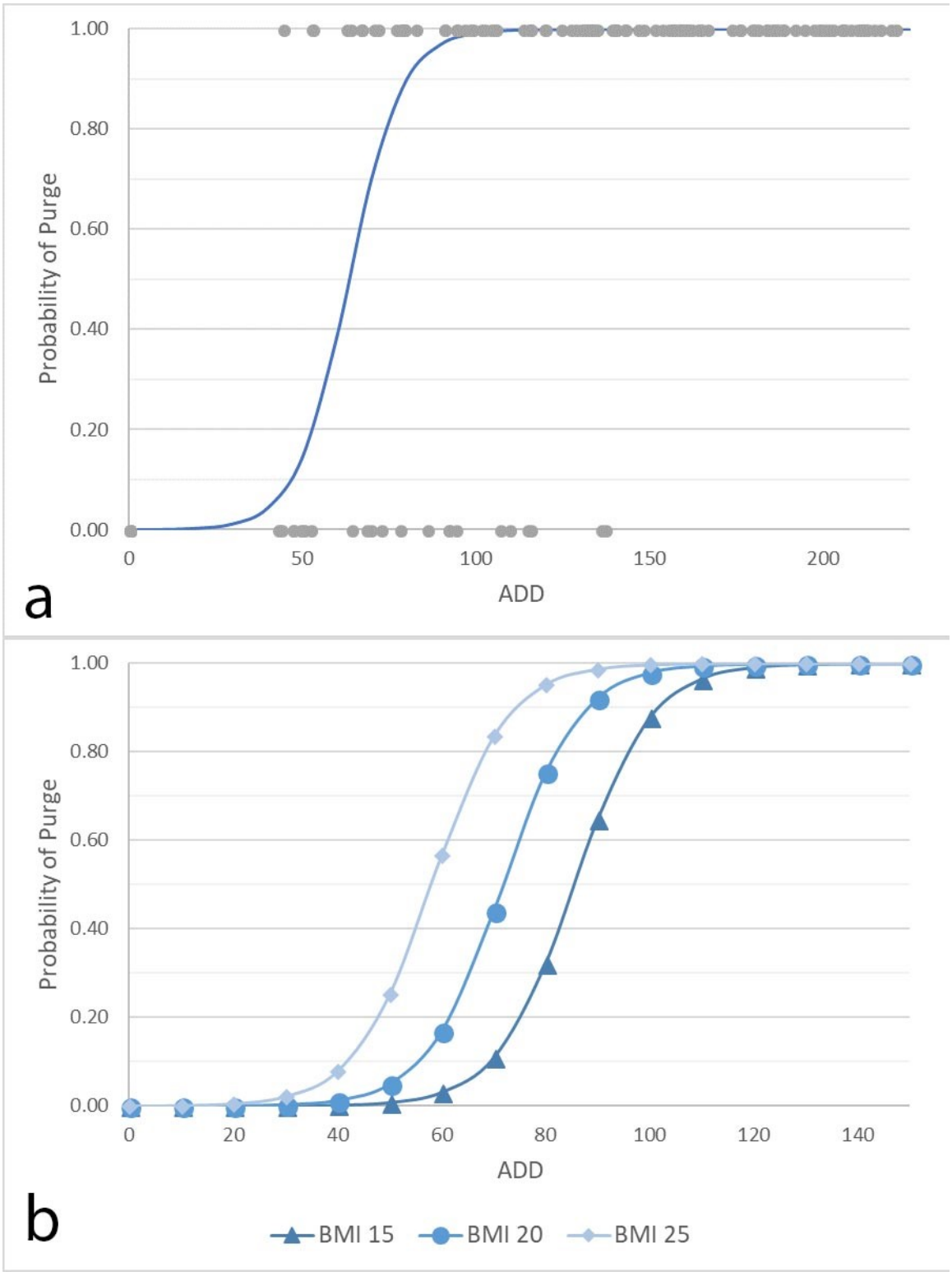

Figure 10. Prediction Curves for Probability of Purge. (a) Probability of purge given ADD using PM1, (b) Probability of purge given ADD using PM2 for three values of BMI (15, 20, 25).

one individual with an infection was included in the final sample. None of the differences were statistically significant.

Two mixed effects models were constructed for purge. In purge model 1 (PM1), ADD was the only fixed effect. The final formula for PM1 is:

$$Probability_{purge} = logit^{-1}(6.680 + (8.650 * scaled\ ADD))$$

Although there was no significant difference in timing of purge between BMI classes, a purge model including BMI (PM2) had a slightly better fit. The final formula for PM2 is:

$$Probability_{purge} = logit^{-1}(6.460 + (8.880 * scaled\ ADD) + (2.230 * scaled\ BMI))$$

Simulated data was then used to construct curves using PM1 and PM2 to predict probabilities of purge having occurred on or before any given ADD. PM1 is presented in Figure 10a along with the original data used to construct the model, while PM2 is presented in Figure 10b for three different values of BMI (one underweight, one normal weight, and one just overweight).

Facial Bloat

Visualizations of the relationship between intrinsic variables and the average timing of facial bloat are available in Appendix A. The data demonstrate a slight negative relationship between BMI and timing of first observed facial bloat; facial bloat occurs slightly earlier in individuals with higher BMIs (see Appendix A, Figure A2). Facial bloat also occurred earlier in individuals with trauma than in individuals without trauma (see Appendix A, Figure A11). There was no observed difference between timing of facial bloat in individuals with or without cancer (see Appendix A, Figure A9), and again, the effect of infection status could not be explored due to the small sample size (n=1) of the group with infection.

Table 6. Comparison of Mean ADD to First Observed Facial Bloat

Grouping	Group	n	Mean ADD	Test Used	Test Statistic	p-value
Sex	Male	15	96.14	Parametric	3.39	***0.004***
	Female	5	65.79			
BMI Class	Underweight	5	102.13	Parametric	2.436	0.102
	Normal	7	99.53			
	Overweight	5	71.22			
	Obese	3	69.20			
Cancer	Cancer-Free	13	91.33	Parametric	-0.176	0.866
	Cancer	6	88.52			
Trauma	No Trauma	16	91.99	Nonparametric	20	0.277
	Trauma	4	74.79			

To explore the significance of these relationships, the means of each group were statistically compared (Table 6). The data was determined to have a normal distribution. The variances of sex, BMI class, and cancer groups were homogeneous and parametric tests were used. The nonparametric Mann-Whitney U-test was used to compare trauma groups, which had heterogenous variances. Individuals with and without infection could not be reliably compared, as only one individual with an infection was included in the final sample. Differences in BMI class, cancer, and trauma means were not significant. The mean ADD to first observed facial bloat of the male and female groups were significantly different.

Two mixed effects models were constructed for facial bloat. In facial bloat model 1 (FBM1), ADD was the only fixed effect. The final formula for FBM1 is:

$$Probability_{facial\ bloat} = logit^{-1}(2.350 + (6.447 * scaled\ ADD))$$

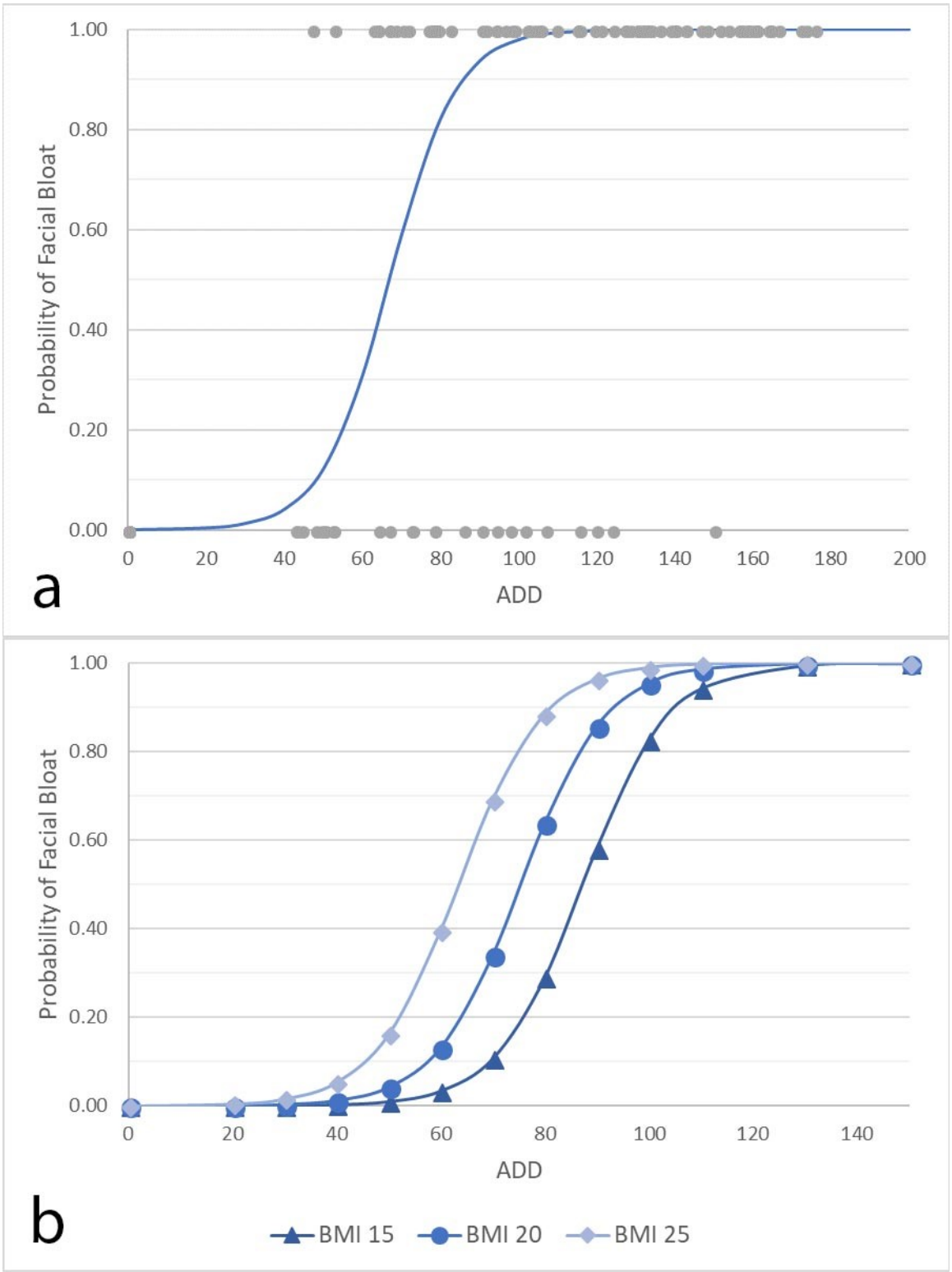

Figure 11. Prediction Curves for Probability of Facial Bloat. (a) Predicted probability of facial bloat given ADD using FBM1, (b) Probability of facial bloat given ADD using FBM2 for three values of BMI (15, 20, 25).

Although there was no significant difference in timing of facial bloat between BMI classes, a model including BMI (FBM2) had a slightly better fit. The final formula for FBM2 is:

$$Probability_{facial\ bloat} = logit^{-1}(2.266 + (6.781 * scaled\ ADD) + (1.742 * scaled\ BMI))$$

Simulated data was then used to construct curves based on these models to predict probabilities of facial bloat having occurred on or before any given ADD. FBM1 is presented in Figure 11a along with the original data used to construct the model, while FBM2 is presented in Figure 11b for three different values of BMI (one underweight, one normal weight, and one just overweight).

Abdominal Distention

Visualizations of the relationships between timing of abdominal distention and intrinsic variables are available in Appendix A. The data suggest a slight negative relationship between BMI and timing of first observed abdominal distention, indicating that abdominal distention occurs earlier in individuals with higher BMIs (see Appendix A, Figure A3). The presence of cancer did not appear to affect the timing of abdominal distention, however, there were slight differences observed based on infection and trauma status (see Appendix A, Figures A9-A11). Abdominal distention appears to be delayed in individuals with causes of death related to infection; however, this finding must be interpreted loosely due to the small size of the infection group (n=2).

To explore the significance of these relationships, the means of each group were statistically compared (Table 7). The data did not have a normal distribution, so

nonparametric methods were used to compare means for all groups. There were no significant differences between group means.

Table 7. Comparison of Mean ADD to First Observed Abdominal Distention

Grouping	Group	n	Mean ADD	Test Used	Test Statistic	p-value
Sex	Male	12	102.47	Nonparametric	29	0.543
	Female	6	109.98			
BMI Class	Underweight	5	121.48	Nonparametric	1.55	0.670
	Normal	5	110.92			
	Overweight	5	92.26			
	Obese	3	88.73			
Cancer	Cancer-Free	12	104.78	Nonparametric	36	0.562
	Cancer	5	110.74			
Infection	No Infection	15	103.55	Nonparametric	24	0.205
	Infection	2	128.93			
Trauma	Intact	15	107.73	Nonparametric	18	0.635
	Minor Trauma	3	91.19			

The dataset used for model construction included 169 observations of 27 individuals. One mixed effects model was constructed for abdominal distention, ADM1, in which ADD was the sole fixed effect. The final formula for ADM1 is:

$$Probability_{abdominal\ distention} = logit^{-1}((5.826 + (12.157 * scaled\ ADD))$$

A second abdominal distention model including BMI was attempted but did not significantly improve the model fit. Simulated data was then used with the ADM1 formula to predict the probability of abdominal distention having occurred on or before any given ADD (Figure 12).

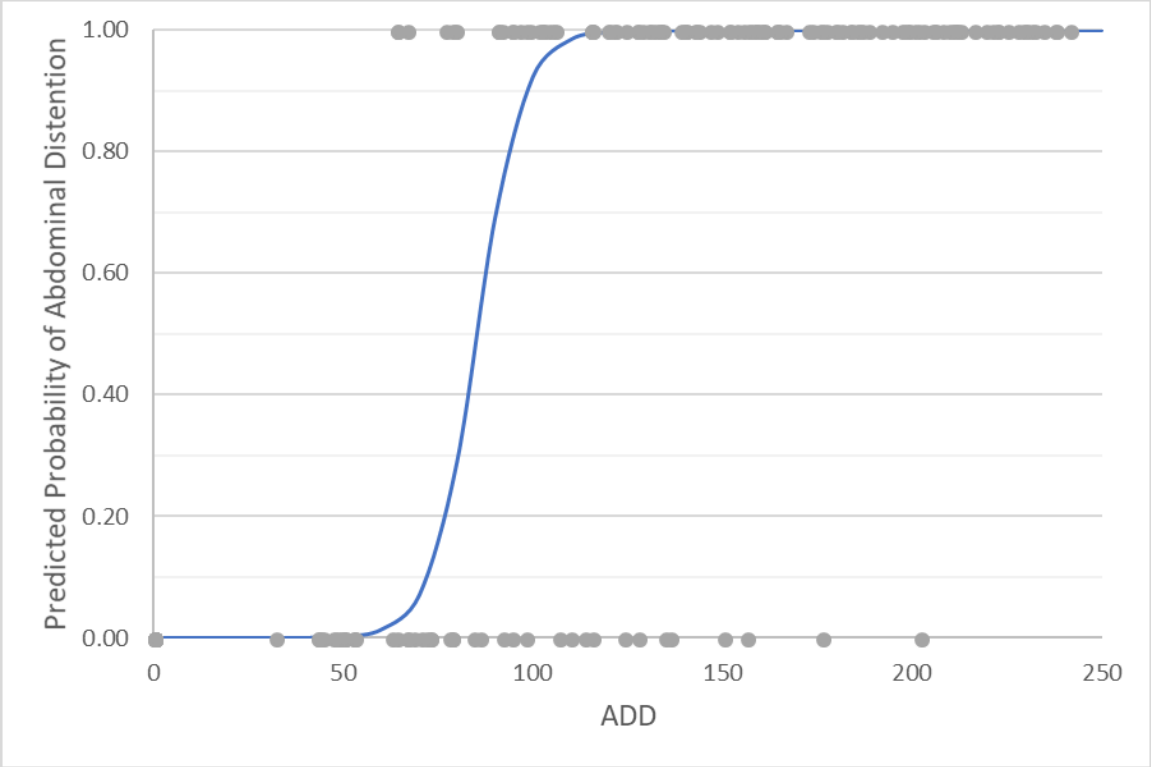

Figure 12. Prediction Curve for Probability of Abdominal Distention. Predicted probability of abdominal distention given ADD using ADM1.

Facial Collapse

Visualizations of the relationship between timing of facial collapse and intrinsic variables are available in Appendix A. These graphs demonstrate a slight positive relationship between BMI and timing of first observed facial collapse, with facial collapse occurring later on average in individuals with higher BMIs (see Appendix A, Figure A4). In addition, facial collapse was delayed in individuals with cancer, and occurred earlier in individuals with infection at the time of death (see Appendix A, Figures A9-A10). Due to small sample size, the relationship between infection and timing of facial collapse should be interpreted cautiously due to the small size of the group with infection (n=2). The timing of facial collapse did not appear to be impacted by the presence of trauma (see Appendix A, Figure A11).

To explore the significance of these relationships, the means of each group were statistically compared (Table 8). The ADD data was normally distributed, and the variances of all compared groups were homogeneous. No significant differences were found between sex, BMI class, cancer, or trauma groups. Individuals who had an infection at the time of death had a significantly different mean ADD to first observed facial collapse than individuals without a reported infection at the time of death.

Table 8. Comparison of Mean ADD to First Observed Facial Collapse

Grouping	Group	n	Mean ADD	Test Used	Test Statistic	p-value
Sex	Male	15	158.10	Parametric	0.941	0.360
	Female	8	145.50			
BMI Class	Underweight	6	136.77	Parametric	0.964	0.43
	Normal	8	156.91			
	Overweight	5	169.88			
	Obese	4	152.55			
Cancer	Cancer-Free	16	142.26	Parametric	1.671	0.145
	Cancer	5	165.46			
Infection	No Infection	19	149.55	Parametric	-2.530	***0.030***
	Infection	2	130.98			
Trauma	Intact	20	153.63	Parametric	0.026	0.982
	Minor Trauma	3	154.28			

The dataset used to construct the mixed effects models for facial collapse included 132 observations from 27 donations. One mixed effects model was constructed for facial collapse, FCM1, in which ADD was the only fixed effect. The final formula for FCM1 is:

$$Probability_{facial\ collapse} = logit^{-1}((3.477 + (8.550 * scaled\ ADD))$$

A second facial collapse model including BMI was attempted but did not significantly improve the model fit. Simulated data was then used with FCM1 to predict the probability of facial collapse having occurred on or before any given ADD (Figure 13).

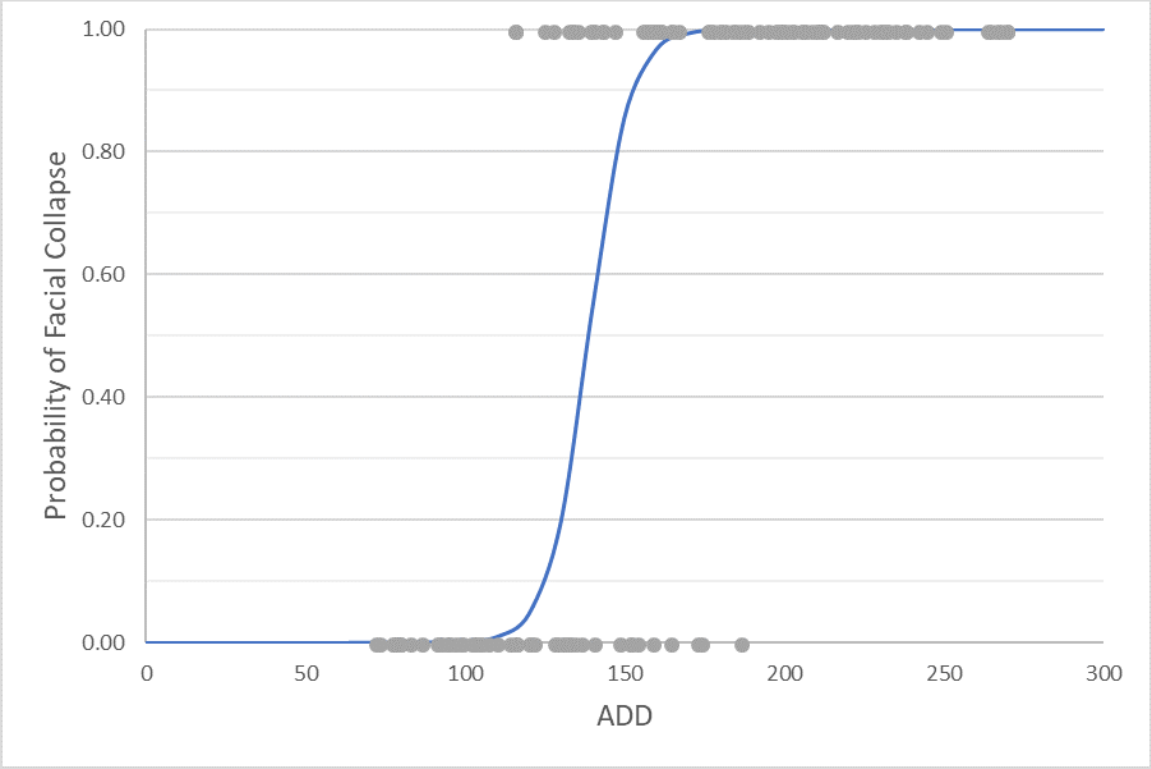

Figure 13. Prediction Curve for Probability of Facial Collapse. Predicted probability of facial collapse given ADD using FCM1.

Abdominal Wrinkle

Visualizations of the relationships between timing of abdominal wrinkle and intrinsic variables are available in Appendix A. A scatterplot suggests a very slight positive relationship between BMI and timing to first observed abdominal wrinkle, while the bar chart indicates a difference between the extreme (underweight and obese) and moderate (normal and overweight) BMI classes (see Appendix A, Figure A5). Abdominal wrinkle was delayed in individuals with cancer (see Appendix A, Figure A9). The effects of infection and trauma could not be explored due to small sample sizes of the group with infection (n=1) and the group with trauma (n=2).

To explore the significance of these relationships, the means of each group were statistically compared (Table 9). The ADD data was normally distributed. For sex and

cancer groups, variances were homogeneous and parametric tests were used. For BMI classes, variances were heterogeneous, and means were compared using a nonparametric test. No significant differences were found between sex or cancer groups, but a significant difference was identified between BMI classes ($\alpha = 0.10$).

Table 9. Comparison of Mean ADD to First Observed Abdominal Wrinkle

Grouping	Group	n	Mean ADD	Test Used	Test Statistic	p-value
Sex	Male	12	172.29	Parametric	0.236	0.823
	Female	3	167.20			
BMI Class	Underweight	3	138.22	Nonparametric	6.769	0.080
	Normal	4	196.42			
	Overweight	5	193.59			
	Obese	3	133.59			
Cancer	Cancer-Free	8	152.76	Parametric	0.980	0.363
	Cancer	5	173.35			

A Dunn Test, used for nonparametric post-hoc analysis, was used to follow up and indicated that a significant difference existed between the overweight and obese BMI classes (Table 10). Substantial but insignificant differences were also noted between underweight-normal, underweight-overweight, and normal-obese pairings, but no difference was noted between normal-overweight and underweight-obese BMI classes. These findings support the observation that the timing of underweight and obese BMI classes different from normal and overweight BMI classes.

Table 10. Dunn Test for Significant Differences in Abdominal Wrinkle Timing

test statistic *p-value*	Normal	Obese	Overweight
Obese	1.830 0.034		
Overweight	-0.117 0.454	-2.021 ***0.022****	
Underweight	1.635 0.051	-0.183 0.428	1.817 0.035

Two mixed effects models were constructed for abdominal wrinkle. AWM1 included only ADD as a fixed effect, and the dataset used to construct it included 86 observations from 20 donations. The final formula for AWM1 is:

$$Probability_{abdominal\ wrinkle} = logit^{-1}(2.104 + (7.362 * scaled\ ADD))$$

Although the relationship between cancer and abdominal wrinkle timing was not significant, AWM2 added cancer as a fixed effect and it dramatically improved the model fit. The dataset used to construct AWM2 included 74 observations from 18 donations, as two donations had an unspecified cause of death and could not be assigned to cancer-free or cancer groups. The final formula for AWM2 is:

$$Probability_{abdominal\ wrinkle} = logit^{-1}(5.035 + (8.460 * scaled\ ADD) - (3.157 * cancer))$$

A third model was attempted, including BMI as a fixed effect, but was discarded because it decreased the model fit. Simulated data was then used to construct curves based on AWM1 and AWM2 to predict probabilities of abdominal wrinkle having occurred on or before any given ADD. AWM1 is presented in Figure 14a along with the original data used to construct the model. AWM2 is presented in Figure 14b, with separate prediction curves for individuals with and without cancer.

Abdominal Collapse

Data visualizations of the relationships between abdominal collapse and intrinsic variables are available in Appendix A. In terms of BMI category, differences in the timing of abdominal collapse appear between extreme (i.e., underweight and obese) and moderate (i.e., normal and overweight) BMI categories (see Appendix A, Figure A6). Collapse was delayed in the cancer group but occurred earlier in the infection

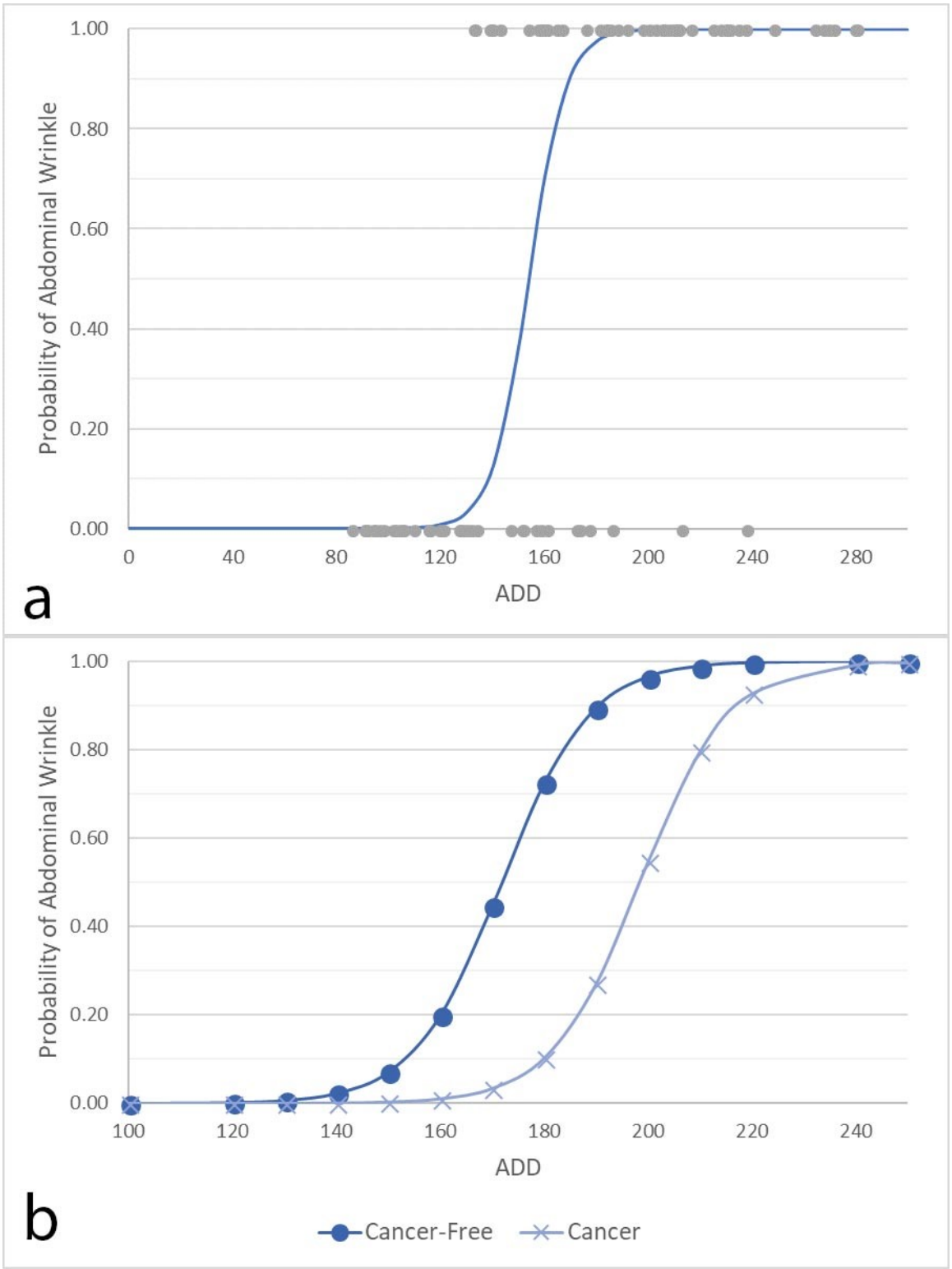

Figure 14. Prediction Curves for Probability of Abdominal Wrinkle. (a) Predicted probability of abdominal wrinkle given ADD using AWM1, (b) Probability of abdominal wrinkle using AWM2, given ADD and cancer status.

and trauma groups (see Appendix A, Figures A9-A11). Due to small sample sizes, the impacts of infection and trauma should be interpreted cautiously.

The means of each group were then statistically compared (Table 11). The ADD data was normally distributed, and the variances of all compared groups were homogeneous; parametric tests were used. None of the groups were significantly different at an alpha-level of 0.05, but the mean ADD to abdominal collapse for the cancer group was significantly different from that of the cancer-free group at an alpha-level of 0.10.

Table 11. Comparison of Mean ADD to First Observed Abdominal Collapse

Grouping	Group	n	Mean ADD	Test Used	Test Statistic	p-value
Sex	Male	13	197.30	Parametric	-0.334	0.747
	Female	6	207.91			
BMI Class	Underweight	6	180.36	Parametric	0.482	0.700
	Normal	7	212.91			
	Overweight	4	217.76			
	Obese	2	184.41			
Cancer	Cancer-Free	13	177.47	Parametric	2.088	0.088
	Cancer	5	237.07			
Infection	No Infection	16	196.53	Parametric	-0.464	0.715
	Infection	2	174.00			
Trauma	No Trauma	15	207.98	Parametric	-1.419	0.195
	Trauma	4	173.18			

Two mixed effects models were constructed for abdominal collapse. ACM1 included only ADD as a fixed effect, and the dataset used to construct it included 113 observations from 27 individuals. The final formula for ACM1 is:

$$Probability_{abdominal\ collapse} = logit^{-1}((5.557 * scaled\ ADD) - 1.545)$$

The relationship between cancer and timing of abdominal collapse was explored in ACM2, which added cancer as a fixed effect, dramatically improving the model fit, with the formula:

$$Probability_{abdominal\ collapse}$$

$$= logit^{-1}(0.489 + (5.701 * scaled\ ADD) - (3.132 * cancer))$$

The dataset used to construct ACM2 included 100 observations from 25 donations, as two donations had unspecified causes of death.

A third and fourth model including BMI and trauma respectively, were attempted but discarded because they failed to improve the model fit. Simulated data was then used to construct curves based on these models to predict the probability of abdominal collapse having occurred. ACM1 is presented in Figure 15a. ACM2 is presented in Figure 15b, with separate prediction curves for individuals with and without cancer.

First Protruding Stain (FPS)

Data visualizations of relationships between the timing of FPS and intrinsic variables are available in Appendix A. A scatterplot and bar plot indicate a slight negative trend between BMI and timing of FPS (see Appendix A, Figure A7). There was no notable difference between timing of FPS based on cancer status, although stain occurred earlier in individuals with trauma (see Appendix A, Figure A9 & A11). The effects of infection could not be tested due to size of the infected group (n=1).

Table 12. Comparison of Mean ADD to FPS

Grouping	Group	n	Mean ADD	Test Used	Test Statistic	p-value
Sex	Male	14	133.93	Parametric	-0.478	0.642
	Female	8	140.23			
BMI Class	Underweight	5	142.52	Parametric	0.203	0.893
	Normal	8	137.91			
	Overweight	7	132.31			
	Obese	2	127.43			
Cancer	Cancer-Free	14	134.04	Parametric	0.517	0.617
	Cancer	7	141.22			
Trauma	No Trauma	19	140.36	Parametric	-2.304	0.103
	Trauma	3	110.04			

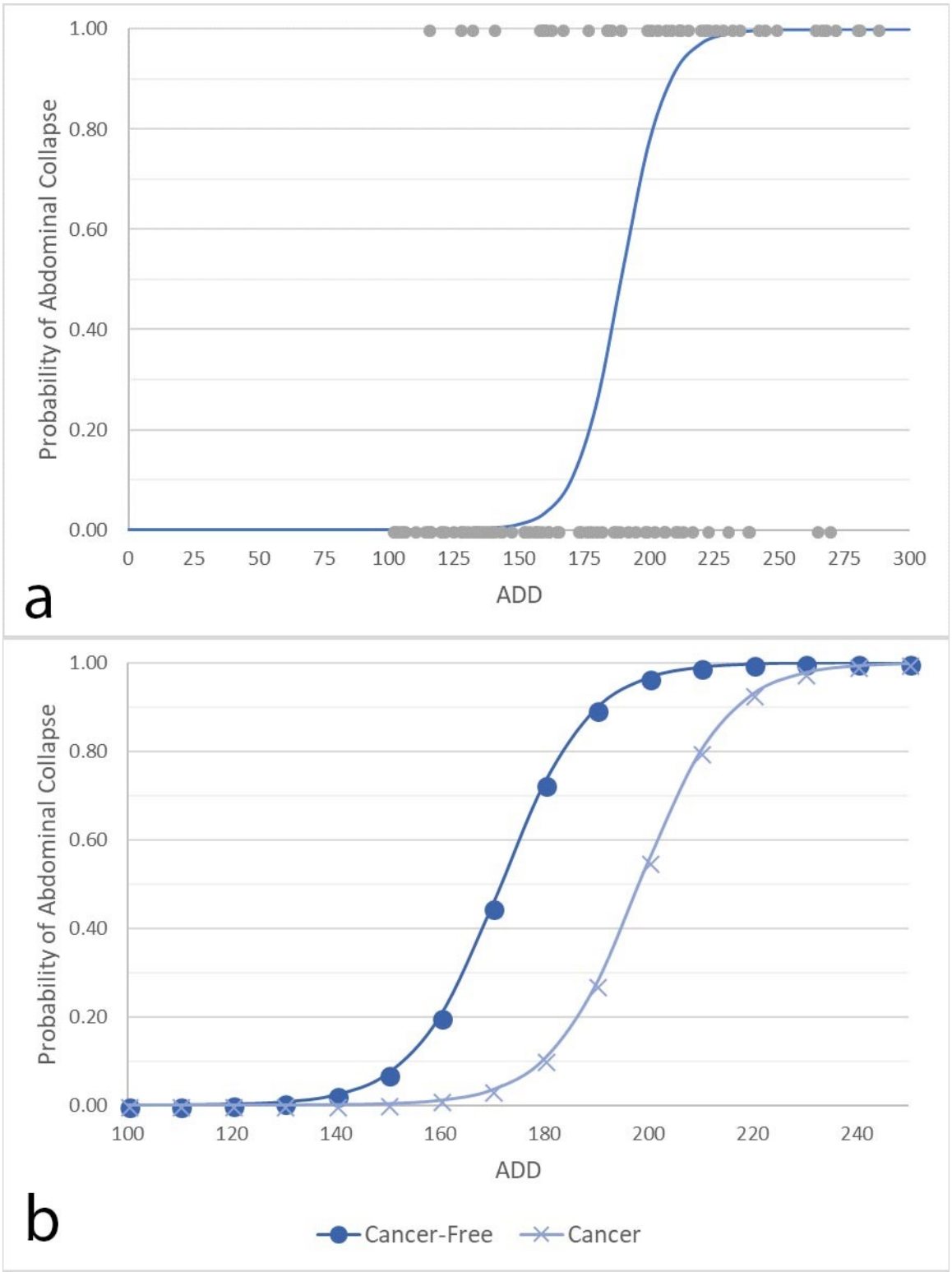

Figure 15. Prediction Curves for Probability of Abdominal Collapse. (a) Predicted probability of abdominal collapse given ADD, generated using ACM1, (b) Probability of abdominal collapse using ACM2, given ADD and cancer status.

The means of each group were then statistically compared (Table 12). The ADD data was normally distributed with homogeneous variances; parametric tests were used. Infection could not be compared because there were no individuals with infection at the time of death in the final sample. There were no significant differences between groups, although a substantial difference was noted between individuals with trauma and individuals without trauma.

One mixed effects model was constructed for FPS. The dataset used for model construction included 137 observations of 27 individuals. Stain model one (SM1) included only ADD as a fixed effect. Models including BMI, cancer, and trauma were attempted but were ultimately discarded when they failed to improve the model fit. The final formula for SM1 is:

$$Probability_{soil\ stain} = logit^{-1}(2.902 + (8.323 * scaled\ ADD))$$

Simulated data was then used with SM1 to construct curves to predict probabilities of FPS having occurred on or before any given ADD. The predicted probability curve of SM1 is presented in Figure 16.

Soil Stain Outline

The soil stain outline differs from the FPS in the distribution of the stain around the remains; the FPS could occur anywhere, whereas the soil stain outline underlies the entire body (see Figures 4 and 5). Data visualizations of the relationship between the timing of soil stain outline and intrinsic variables are available in Appendix A. A scatterplot and bar chart suggest a slight negative relationship between BMI and timing of stain outline (see Appendix A, Figure A8). Stain outline occurred later in individuals with cancer (see Appendix A, Figure A9). The effects of infection and trauma could not

be evaluated due to small size of the group with infection (n=1) and the group with trauma (n=1).

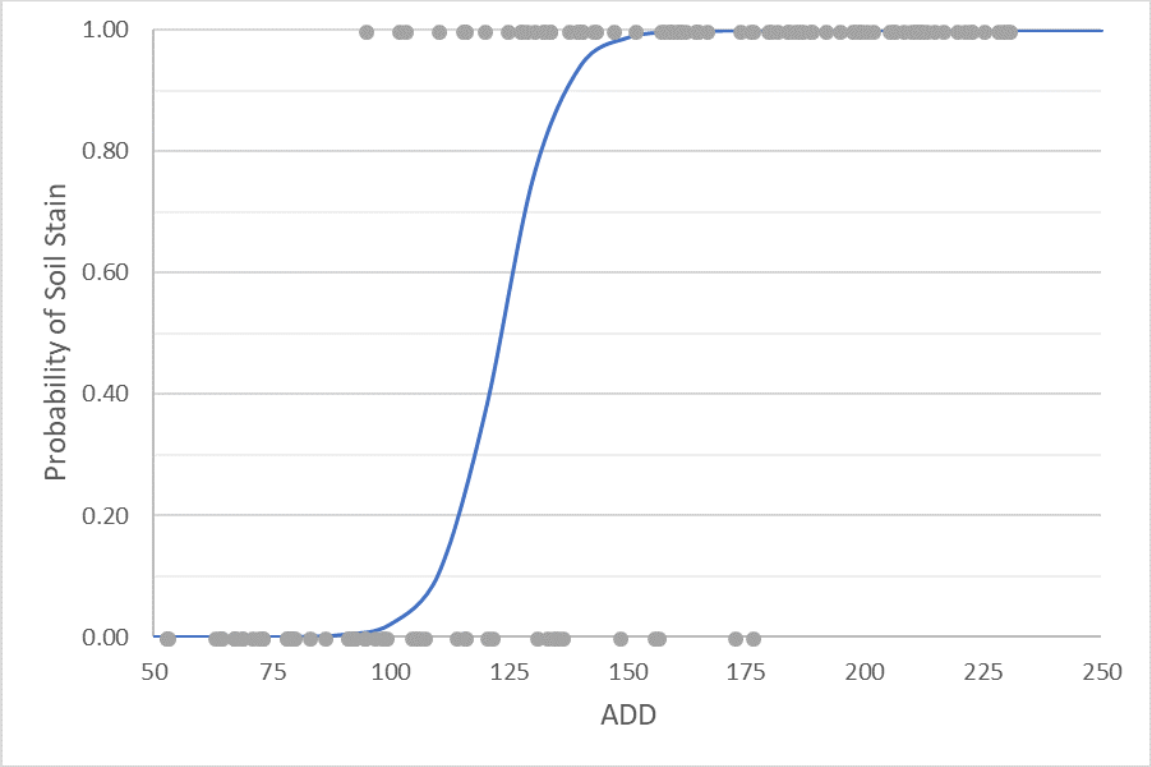

Figure 16. Prediction Curve for Probability of First Protruding Stain. Predicted probability of FPS given ADD, generated using SM1.

Table 13. Comparison of Mean ADD to First Observed Stain Outline

Grouping	Group	n	Mean ADD	Test Used	Test Statistic	p-value
Sex	Male	10	188.63	Nonparametric	21	0.679
	Female	5	211.92			
BMI Class	Underweight	4	187.88	Nonparametric	0.59	0.900
	Normal	5	199.08			
	Overweight	4	212.93			
	Obese	2	173.64			
Cancer	Cancer-Free	11	184.12	Nonparametric	29	0.412
	Cancer	4	230.15			

The means of each group were then statistically compared (Table 13). The ADD data was not normally distributed, so nonparametric tests were used to compare means of

sex, BMI class, and cancer groups. Infection and trauma groups could not be compared because there was only one individual with infection and one individual with trauma and in the final sample. There were no significant differences between groups. Mixed effects models were attempted for stain outline using a subset including 72 observations from 24 donations. However, all attempted models failed to converge due to singularity.

Accuracy of Mixed Effects Models

The results of the preliminary analysis of mixed effect model accuracy are presented in Table 14. The scaled ADD and additional fixed effects from a subset of observations were input into the model formulae to predict whether or not the indicator of interest would be present or absent, with probabilities less than or equal to 50% predicting indicator absence and probabilities greater than 50% predicting indicator presence.

The proportion of correctly predicted observations range from a minimum of 70% in the facial bloat models to 93% in AWM2 for predicting abdominal wrinkle in individuals without cancer. The rate of type I errors, the prediction that an indicator would be present when it was actually absent, ranged from 7% in the AWM2 model to 60% in FBM1. Type II errors, or the observation that an indicator was present although it was predicted to be absent, were generally lower, ranging from 0% in models of abdominal wrinkle and abdominal collapse to 29% in ACM2 when predicting abdominal collapse in individuals with cancer.

Table 14. Error Rates of EDI Mixed Effects Models

	Model	Type I Error Rate	Type II Error Rate	Correct Classification Rate
Purge	PM1	0.29	0.09	0.87
	PM2	0.29	0.13	0.83
Facial Bloat	FBM1	0.60	0.15	0.70
	FBM2	0.50	0.20	0.70
Abd Distention	ADM1	0.20	0.05	0.90
Facial Collapse	FCM1	0.20	0.20	0.80
Abdominal Wrinkle	AWM1	0.17	0.00	0.77
	AWM2			
	cancer-free	0.07	0.00	0.93
	cancer	0.33	0.00	0.80
Abdominal Collapse	ACM1	0.22	0.25	0.77
	ACM2			
	cancer-free	0.30	0.00	0.80
	cancer	0.25	0.29	0.73
Protruding Stain	SM1	0.09	0.16	0.90

IV. DISCUSSION

This project addressed three key questions:

1. Are sequential, visually-observable indicators of early decomposition related to bloat, purge, and collapse available to characterize and refine PMI estimations?
2. Do intrinsic variables such as sex, body size, cause of death, or bodily trauma impact the timing of these EDIs?
3. Can the probability of these EDIs having occurred be modeled accurately given accumulated degree days and/or relevant intrinsic variables?

With regards to the first of these questions, this project identified eight EDIs that encompass the period from death to collapse: purge, first protruding soil stain, facial bloat, abdominal distention, facial collapse, abdominal wrinkle, abdominal collapse, and soil stain outline. Several of these indicators are reliably sequential due to their related nature: facial bloat is always succeeded by facial collapse, while abdominal distention is followed by abdominal wrinkle and/or abdominal collapse. This is not to say that each indicator occurs in every case, as decomposition can take several alternative trajectories depending on environmental circumstances. However, the point remains that no known research to date has observed the natural reinflation of remains once collapse has occurred.

Visual indicators of purge and soil staining were less consistent in their timing. Generally, purge was first observed around the time of facial bloat, with first protruding soil stain appearing shortly thereafter. The appearance of a full stain outline was highly variable, but often occurred during the deflation of the abdomen when the integrity of the remains was compromised, allowing for rapid leaching of fluids into the surrounding soil.

Overall, higher variability in the timing of indicators was noted for those that occur later in the decomposition process, such as abdominal wrinkle, abdominal collapse, and soil stain outline. This variability may reflect a transition from decomposition driven primarily by the metabolic processes of enteric microorganisms, which may be expected to occur at predictable rates based on temperature in a "controlled" internal environment, to decomposition that is influenced by an increasingly complex suite of interacting external variables, including invertebrate activity. As the physical barriers between the remains and the external environment are broken down, the decomposition process is increasingly susceptible to variation introduced by features of the microenvironment, including the biological organisms present, the relationships between them, and the abiotic variables that influence their activities.

This project focused on explaining variation in the decomposition attributed to intrinsic variables expected to influence the structure of the enteric microbial community. Intrinsic variables, however, appear to have limited effects on the timing of all EDIs. Exploratory data analysis identified several general trends. While statistical comparison of group means demonstrated that the differences observed were seldom significant at or above a 90% confidence interval, the validity of these comparisons were limited by the small sample size of some of the groups. In particular, donations with causes of death related to infection and donations with bodily trauma were underrepresented in the overall sample. Expanding the sample used for these comparisons may reveal significant trends that were missed by this analysis, which included observations from a maximum of 30 donations.

There were no significant differences in the mean ADD to first observation of purge, abdominal distention, protruding stain, or stain outline for any intrinsic variable groups. A significant difference was noted between the mean ADD to first observation of facial bloat in males and females, with facial bloat observed earlier in females. This may be due to sampling error, as only five females were compared to fifteen males. There were no significant differences between the sexes for any other indicator in this study. A comparison of mean ADD to facial collapse in donations with causes of death related to infection and donations with unrelated causes of death also yielded a significant difference, with the infected group collapsing earlier than the noninfected group. As before, the significant difference is likely due to sampling error, as the infected group was comprised of only two individuals.

In terms of body mass and composition, EDIs which occur during bloat and purge (active purge, facial bloat, abdominal distention, and soil staining) occurred earlier in individuals with higher BMIs. Interestingly, the effects of BMI differed for EDIs that occur during collapse (facial collapse, abdominal wrinkle, and abdominal collapse). Facial collapse occurred earlier in lower BMI categories, while abdominal wrinkle and collapse occurred earlier in groups with more extreme BMIs (i.e., underweight and obese). Significant differences were noted only between BMI classes for abdominal wrinkle, with post-hoc analyses revealing that the significant differences occurred between overweight and obese BMI classes.

Although it's possible that this could be due to sampling error, an alternative explanation could involve the relationship between carcass size and the colonization of invertebrate larvae, which have been shown to play a critical role in driving collapse by

compromising the integrity of the surrounding tissue (Pechal et al. 2014). Smaller carcasses support a limited number of larvae but can quickly be consumed, so tissue integrity is compromised earlier. Larger carcasses support larger numbers of larvae, but may take longer to consume. Extremely large carcasses, however, have heavy layers of tissue overlying the abdomen. The weight of these tissue layers could apply external force that limits the amount of gas that can accumulate within the body, leading to an increased rate of purge and an accelerated collapse.

The timing of abdominal collapse appeared to be affected by whether cause of death was attributed to cancer, although this difference was only significant within a 90% confidence interval. On average, the cancer group showed delayed timing of abdominal collapse compared to the cancer-free group. This could be related to the influence of cancer or cancer treatment on microbial communities. Increasing evidence suggests that microbial communities play a substantial roll in attracting necrophagous invertebrates to decomposing remains using a form of chemical communication known as quorum-sensing (Liu et al. 2016; Mohr and Tomberlin 2014; Tomberlin et al. 2012). If the enteric microbial community is disrupted prior to death, invertebrate colonization of remains may be delayed, prolonging bloat and thus delaying collapse (Pechal et al. 2014). Finally, substantial but insignificant differences in the timing of FPS were noted between donations with and without minor bodily trauma. On average, soil stains appeared under remains with minor bodily trauma earlier than remains that were intact. The compromised integrity of remains with trauma would likely allow purging fluids to escape from the body sooner after death and in greater quantities. Although this trend was

not statistically significant, this could once again be due to the small sample size of individuals with trauma.

The mixed effects models developed show promise. Preliminary assessments demonstrate reasonable levels of accuracy in predicting indicator presence or absence based on ADD. However, the models were tested using observations that were used in their construction; consequently, their accuracy in modeling observations of new individuals has yet to be tested. Models including a fixed effect for cancer, specifically AWM2 and ACM2, improve overall prediction capacity substantially but have fairly high type I and type II error rates in the cancer-specific model. This suggests that while cancer does have an impact on the timing of abdominal wrinkle and abdominal collapse, greater sample sizes are needed to adequately model the variation within these groups.

There is plenty of work yet to be done in the field of early decomposition taphonomy. This research has now identified and defined several EDIs, but the intraobserver and interobserver error in identifying these indicators requires attention to verify their ease-of-use in practical contexts. Although indicators were designed to promote objective identification from both the field and standard photographic documentation, the congruency of identifying indicators *in situ* versus retrospectively should also be evaluated to confirm that combining and comparing *in situ* and retrospective data is valid.

Slight differences in the timing of indicator appearance were noted between groups with and without infection, with and without cancer, and with and without bodily trauma. Unfortunately, sample sizes were too small to statistically verify these trends. Future research will focus on expanding the sample to incorporate as much of the

retrospective data available from the Texas State Willed Body Donation Program as possible, focusing on these target groups and including a new group to assess variation in indicator timing introduced by external variables such as animal scavenging events or season of placement. Expanding the sample will also enable the construction of improved mixed effects models that account for additional individual-level variation. The sample size for this study prevented accurate estimation of coefficients in models with more than two fixed effects, but more complex models may be developed as additional data is incorporated into the analysis.

V. CONCLUSION

The EDIs identified here aim to reduce the subjectivity in the analysis of human remains. The eight indicators are relatively consistent in appearance and are usually observed at some point in the early decomposition process, the timing of their occurrence demonstrates the tremendous variability in the rate and pattern of human decomposition. Some of the indicators are strongly sequential due to their interrelated nature (i.e., facial bloat is always followed by facial collapse, never vice versa), allowing them to be used for PMI estimation with minimal concerns of trait reversal or reappearance. Others, such as purge, FPS, and soil stain outline, occur with more variable timing relative to other EDIs.

This project evaluated potential relationships between the timing of these indicators and intrinsic variables, or those that are specific to an individual set of remains, including body mass index, cause of death, and the presence of bodily trauma. While sample sizes were too small to statistically verify the influence of most of these variables, a common problem in taphonomic research that utilizes human remains, general trends were identified and the nature of the indicators allow for the sample to be expanded retrospectively using photographic documentation of human remains with known postmortem intervals.

Despite the small sample size, the mixed effects models constructed to predict indicator presence or absence from ADD show potential with accuracy of 70-93%. Future work will focus on more robust testing of model accuracy and, once additional data has been collected, improving model fit through the inclusion of new variables. Ultimately, the models may be transformed to predict ADD intervals from the combinations of

indicators that are present, making it a useful medicolegal tool for the evaluation of postmortem interval in human remains that are found in the early decomposition period.

APPENDIX SECTION

Appendix A

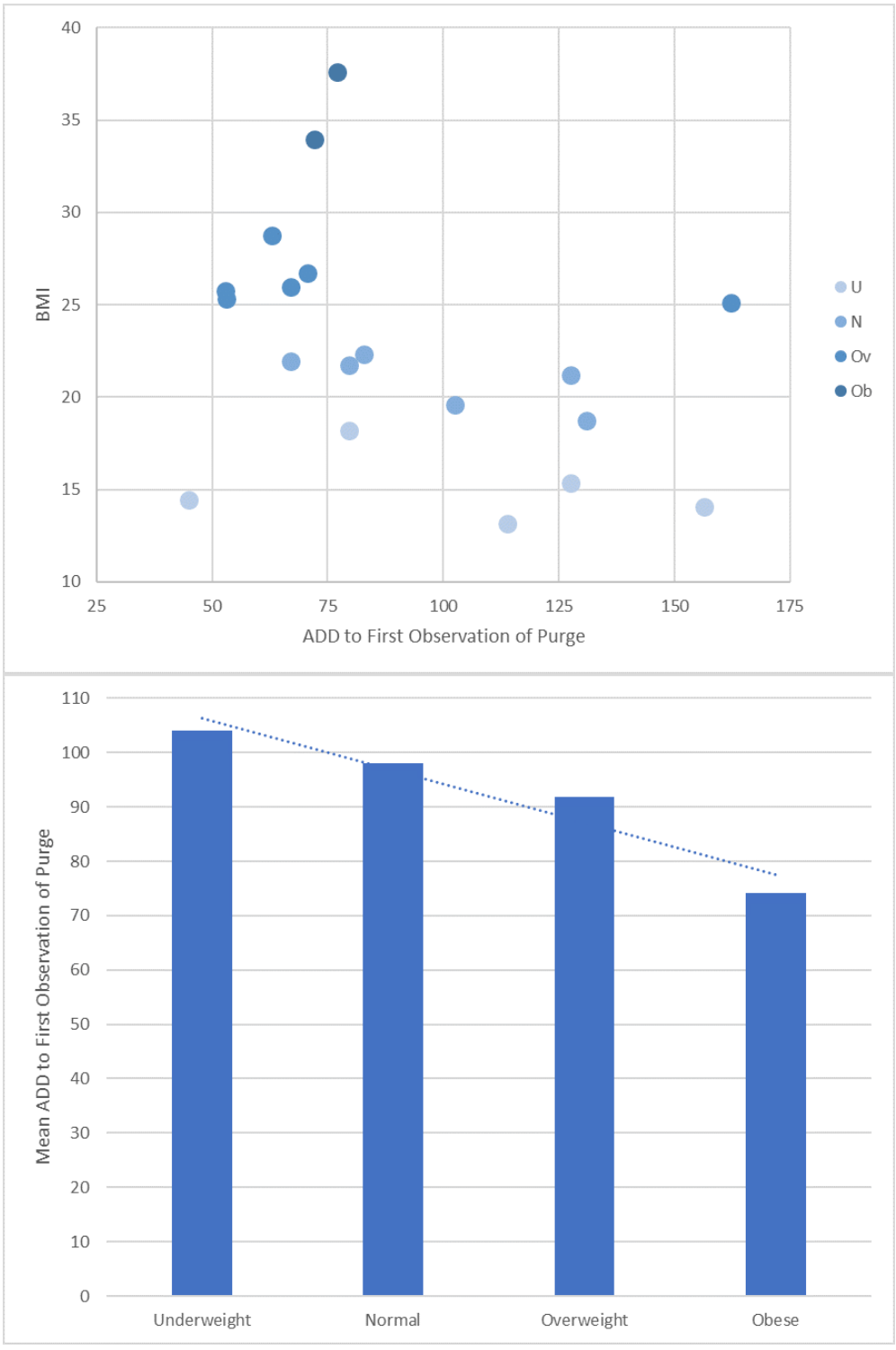

Figure A1. Relationship between BMI and ADD to First Observed Purge.

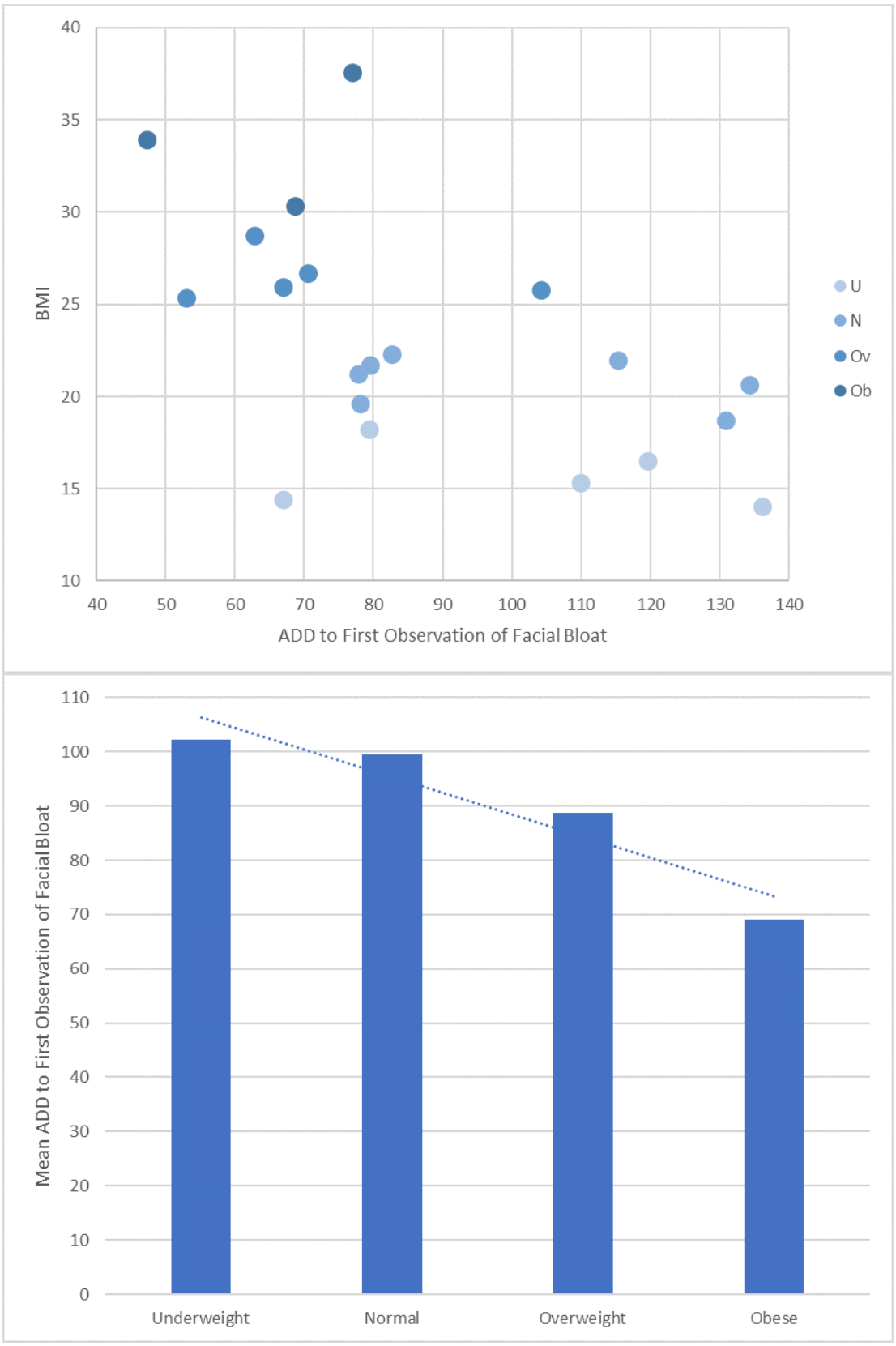

Figure A2. Relationship between BMI and ADD to First Observed Facial Bloat.

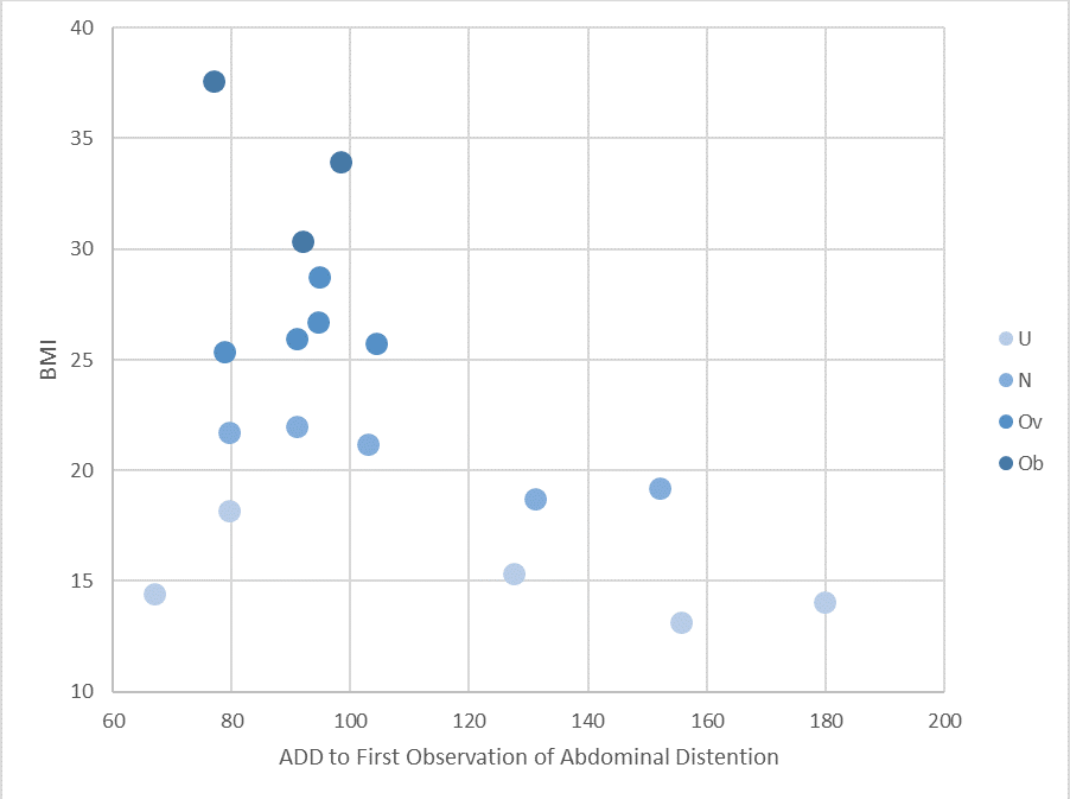

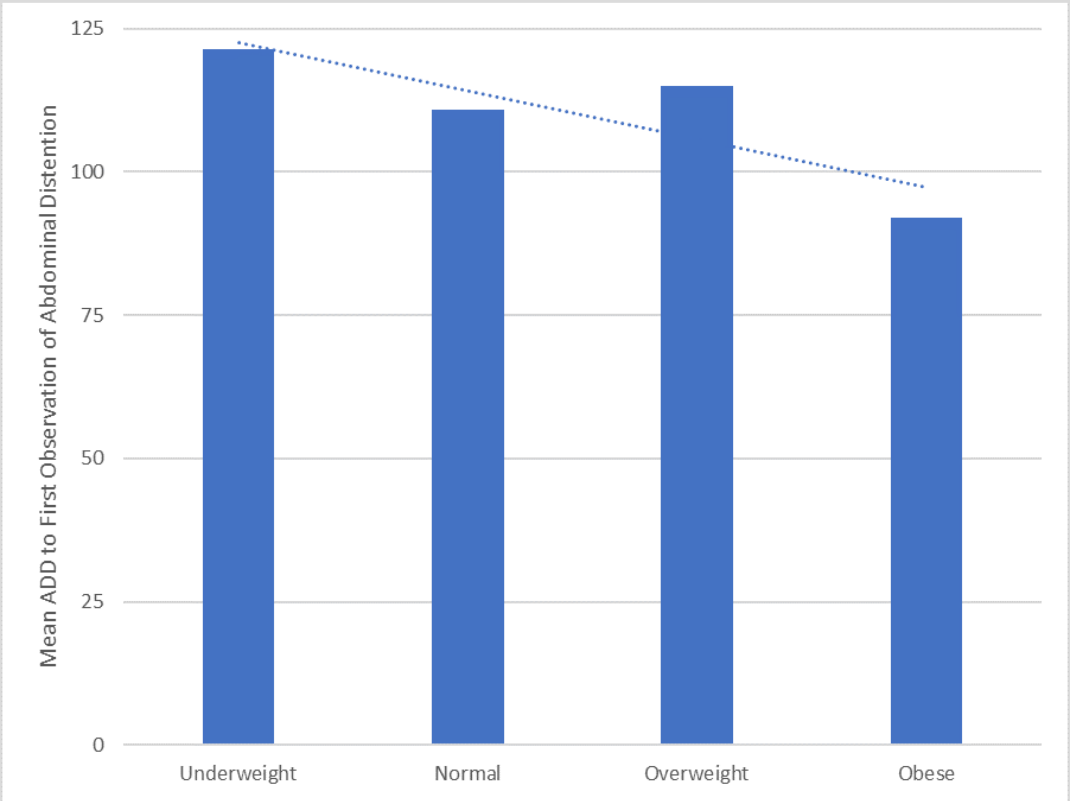

Figure A3. Relationship between BMI and ADD to First Observed Abdominal Distention.

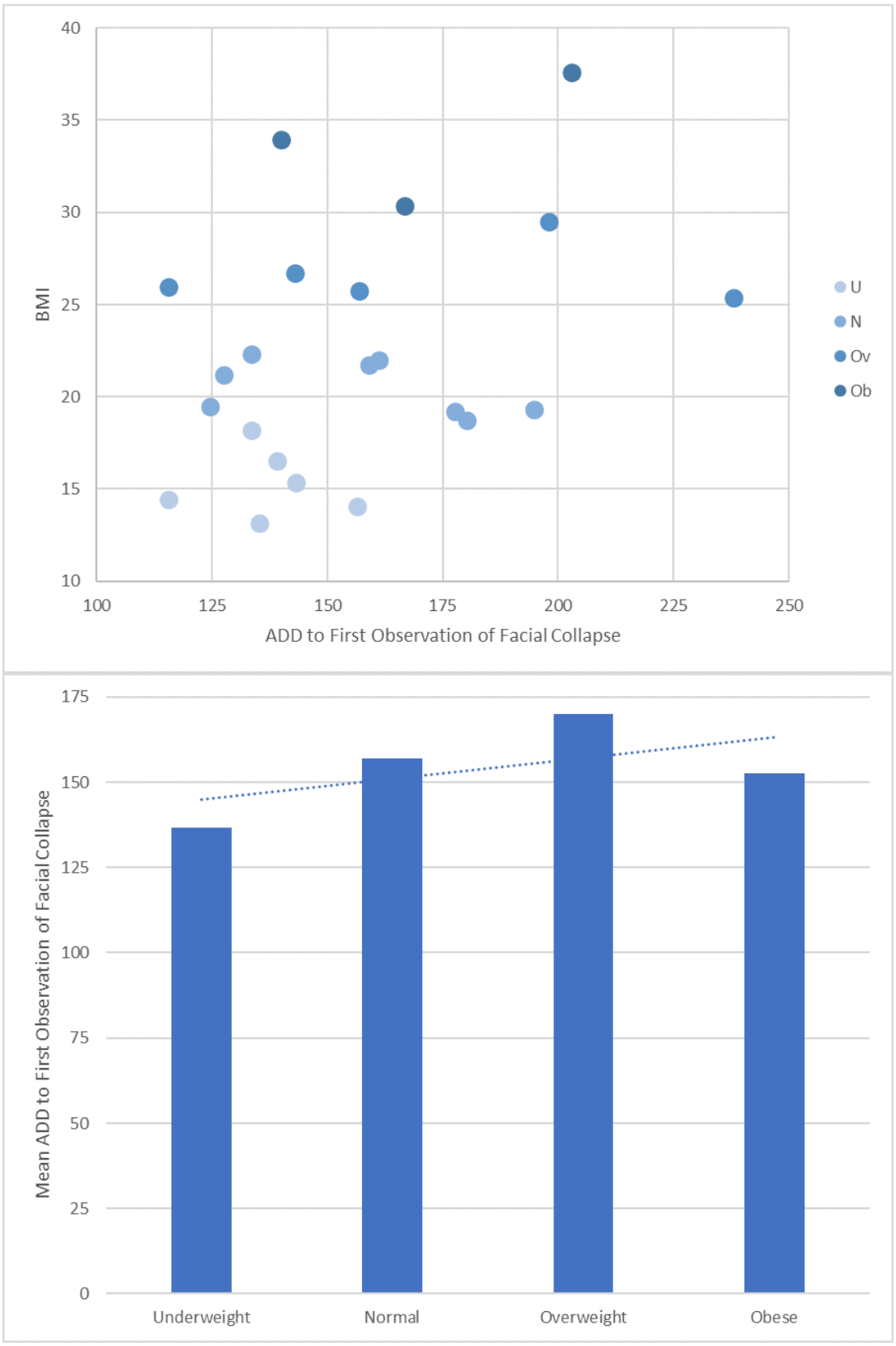

Figure A4. Relationship between BMI and ADD to First Observed Facial Collapse.

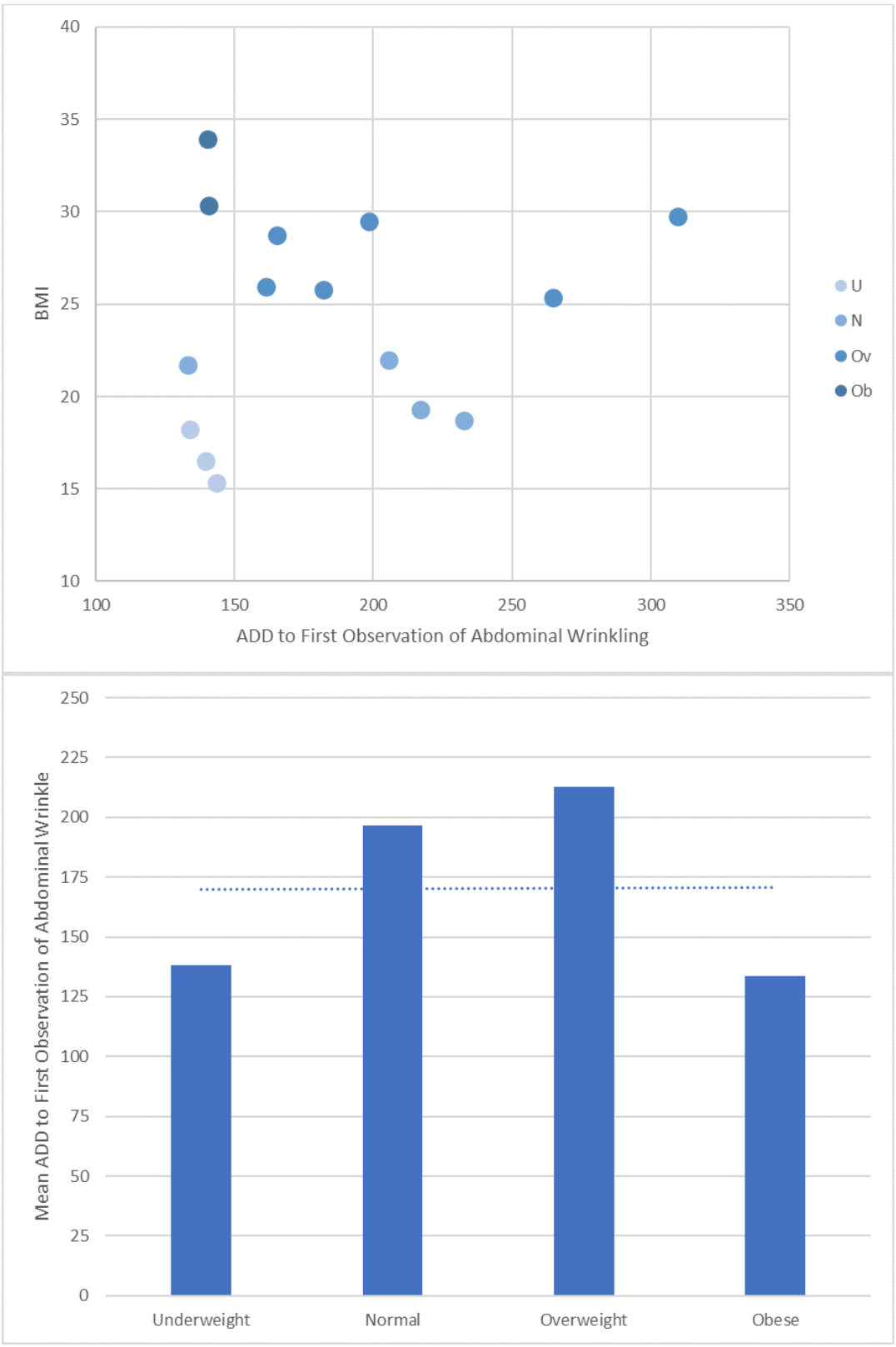

Figure A5. Relationship between BMI and First Observation of Abdominal Wrinkle.

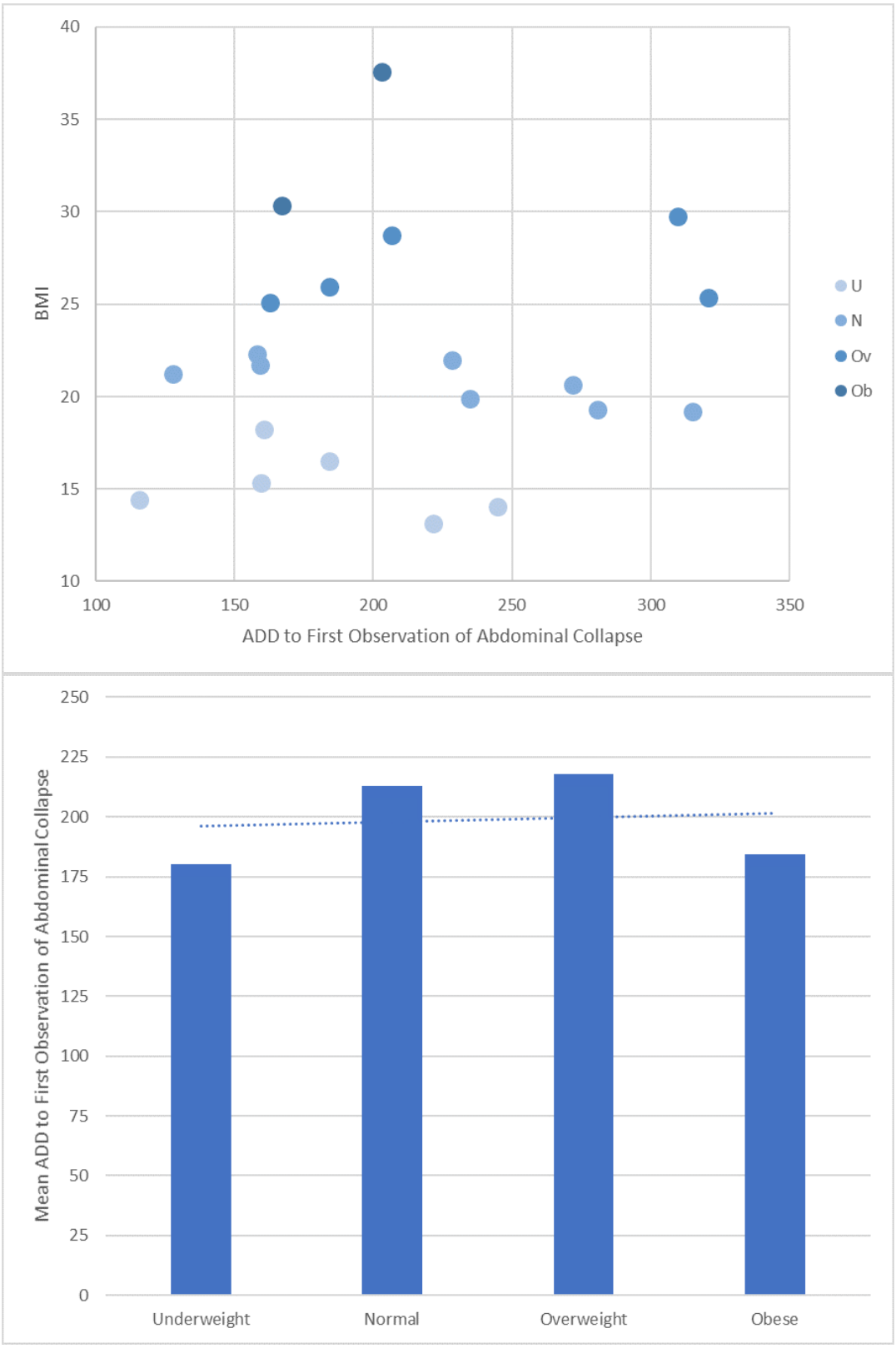

Figure A6. Relationship between BMI and First Observation of Abdominal Collapse.

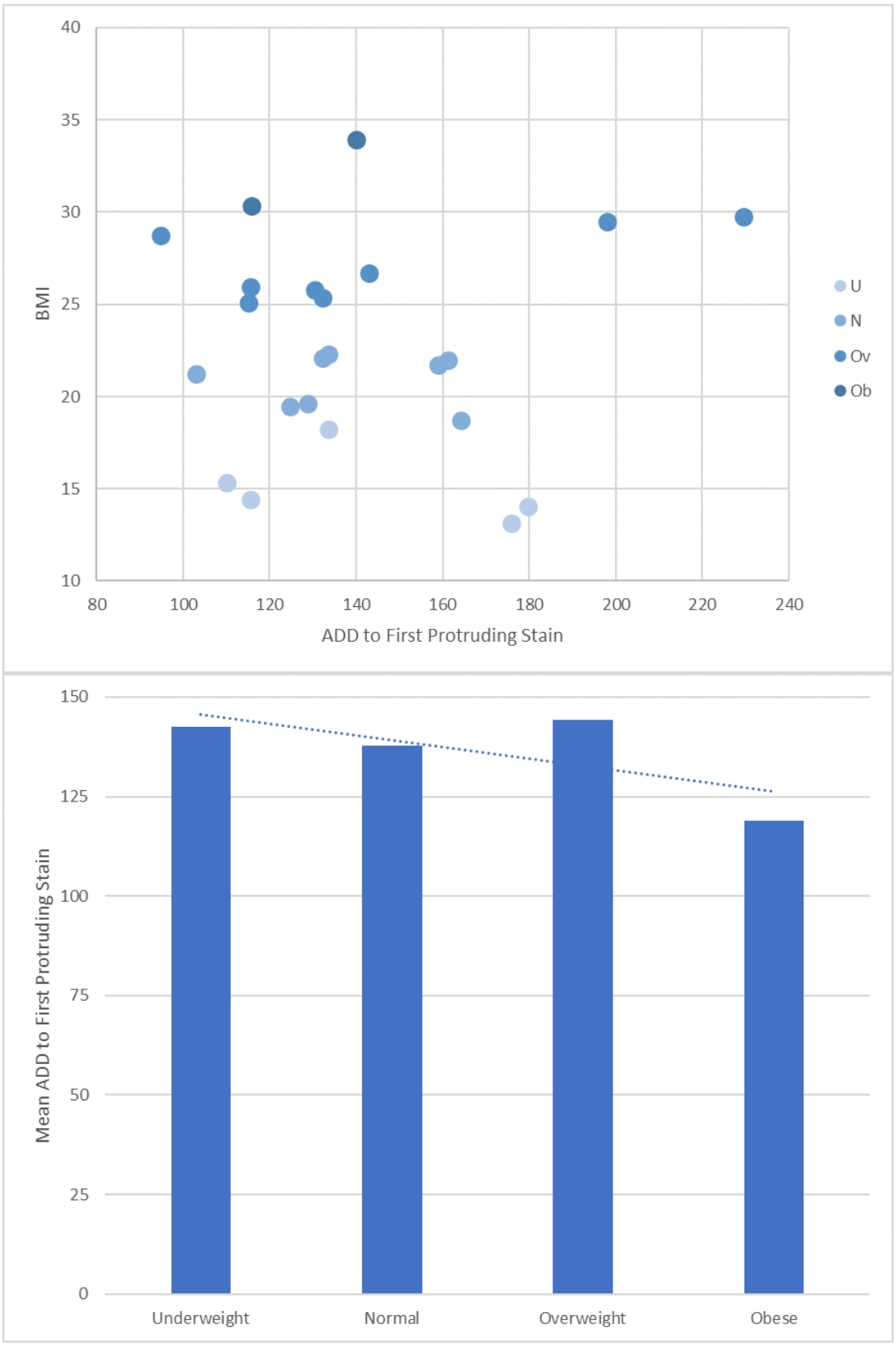

Figure A7. Relationship between BMI and ADD to FPS.

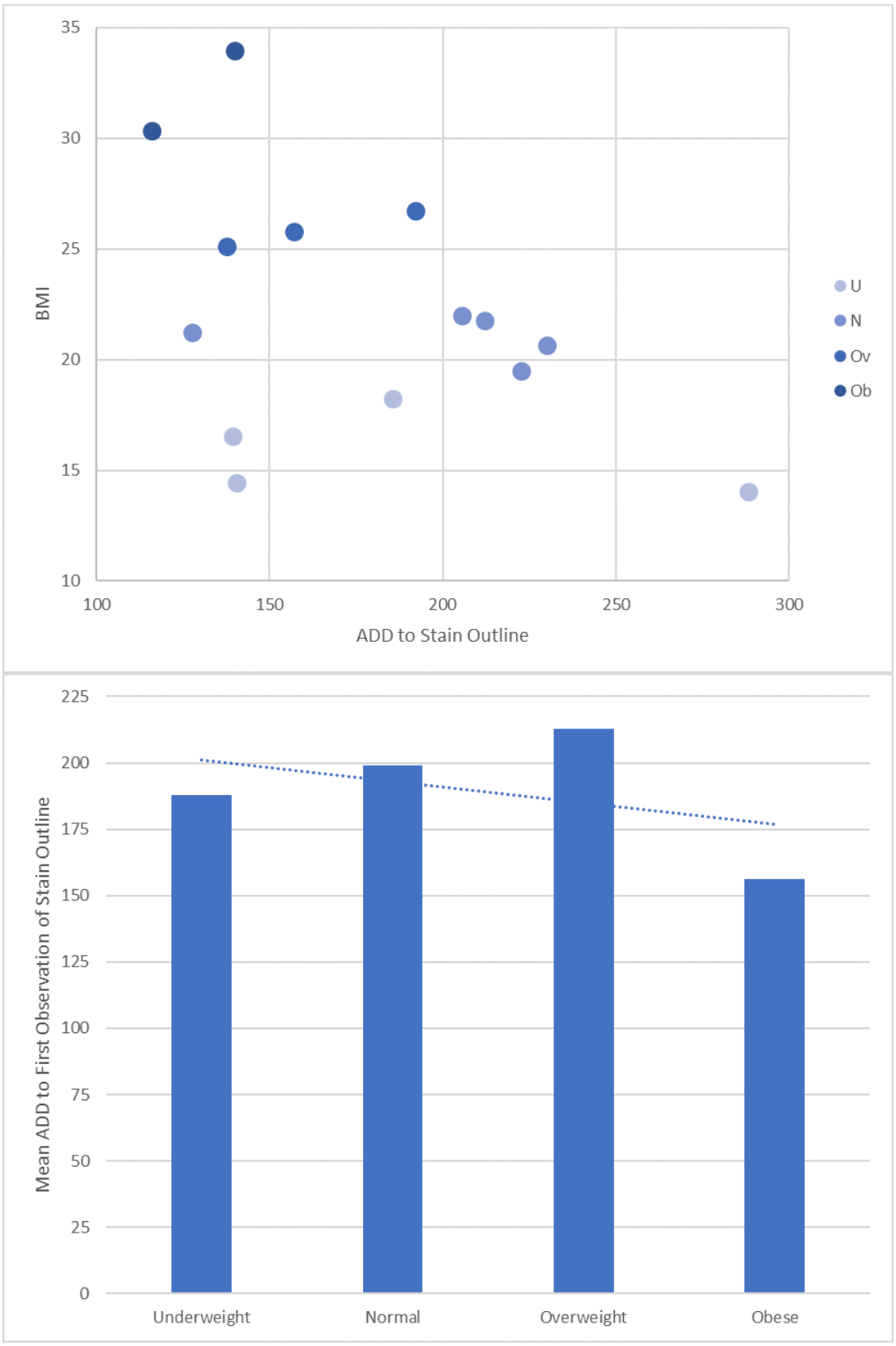

Figure A8. Relationship between BMI and First Observation of Stain Outline.

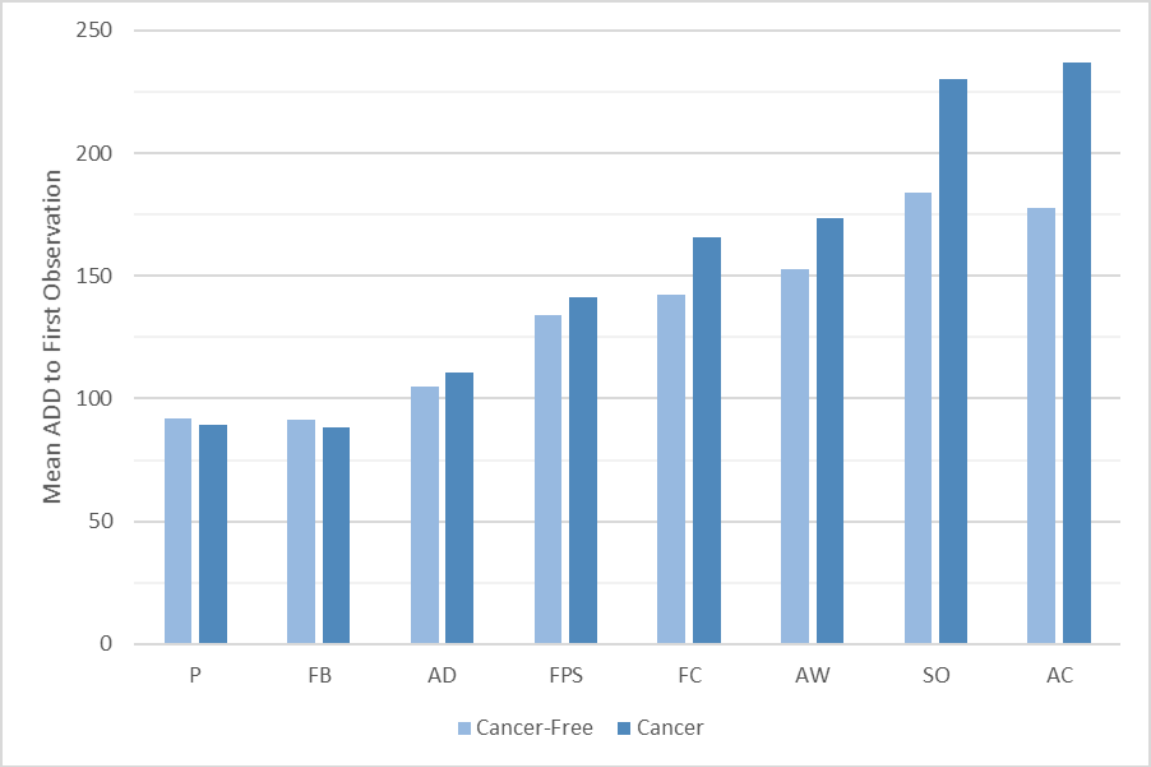

Figure A9. Mean ADD to First Observation of EDIs by Cancer Status.

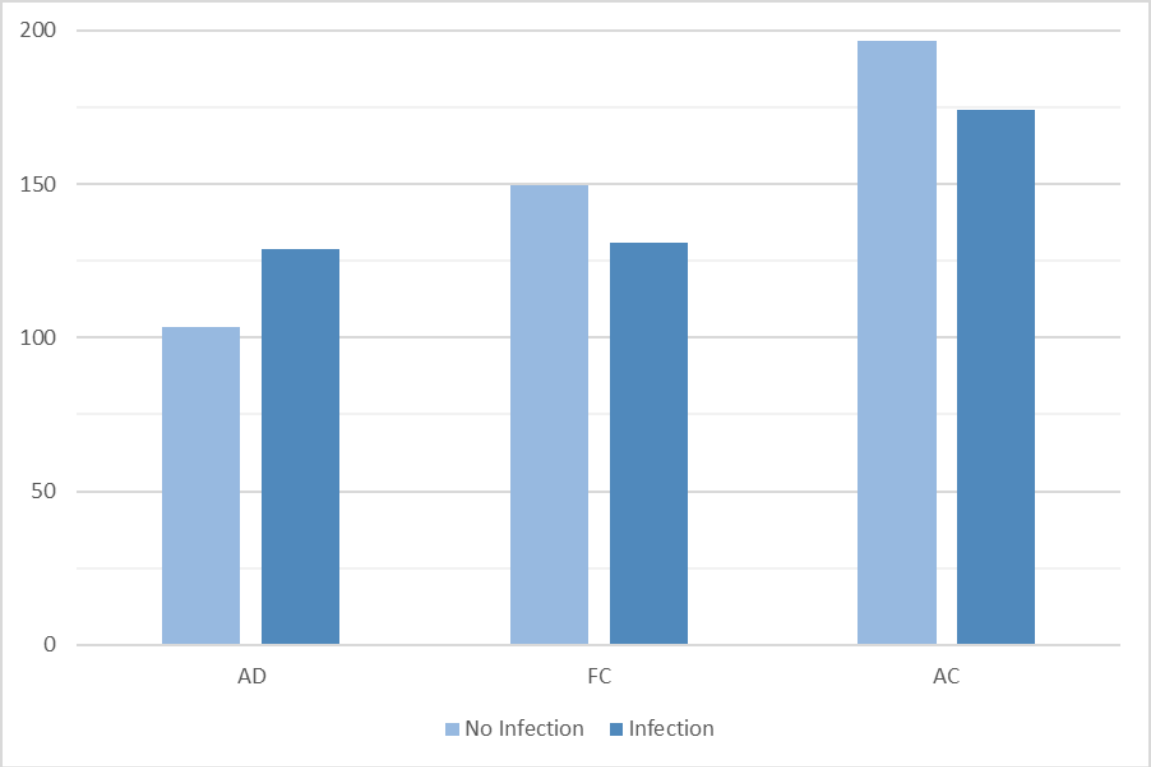

Figure A10. Mean ADD to First Observation of EDIs by Infection Status.

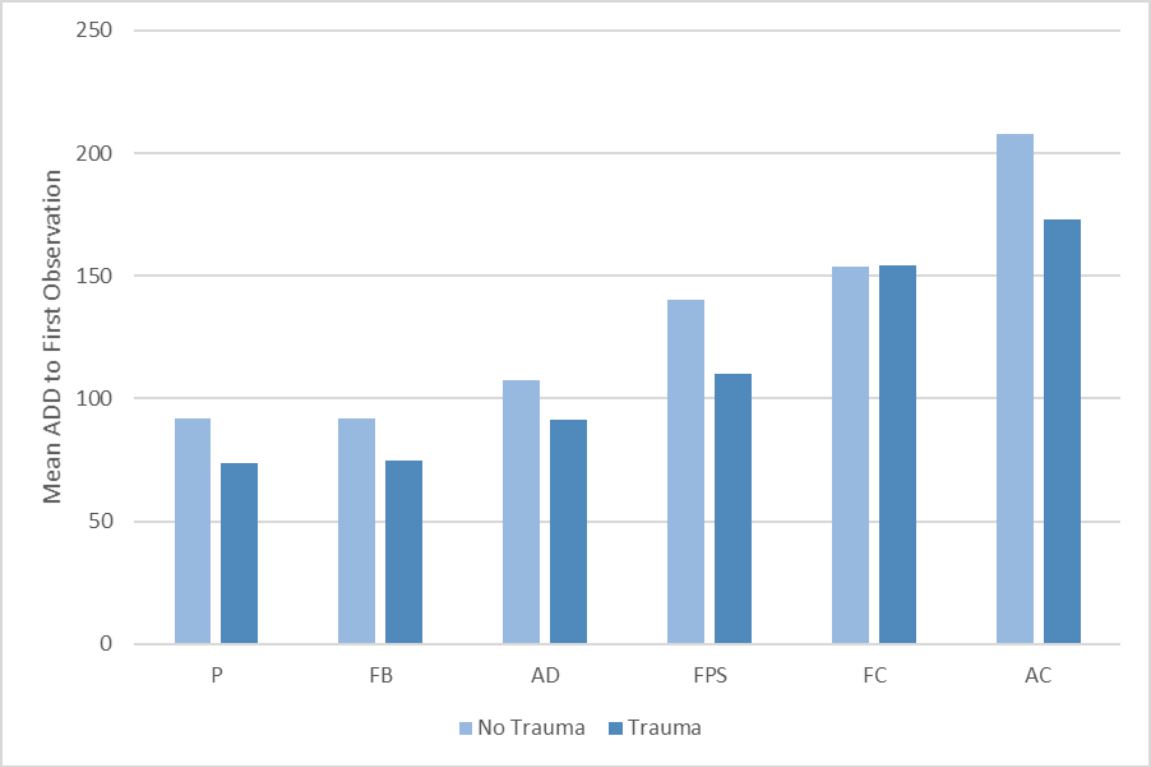

Figure A11. Mean ADD to First Observation of EDIs by Trauma Status.

Appendix B

Table B1: Scaling of Continuous Variables by EDI

EDI	Scaled ADD	Scaled BMI
Purge	$\frac{\text{ADD} - 114.157}{65.525}$	$\frac{\text{BMI} - 21.904}{5.991}$
Facial Bloat	$\frac{\text{ADD} - 87.022}{55.204}$	$\frac{\text{BMI} - 22.843}{5.941}$
Abdominal Distention	$\frac{\text{ADD} - 119.619}{71.752}$	-
Facial Collapse	$\frac{\text{ADD} - 160.553}{53.534}$	-
Abdominal Wrinkle	$\frac{\text{ADD} - 168.836}{51.982}$	-
Abdominal Collapse	$\frac{\text{ADD} - 175.913}{48.386}$	-
First Protruding Stain	$\frac{\text{ADD} - 139.961}{50.201}$	-

Table B2: Prediction Model Formulae Specifications

Model	DIC	Intergroup Variance	Term*	Value	SE	z	p
PM1	-39.0	23.52	Intercept	6.68	2.37	2.82	0.005
			ADD	8.65	2.50	3.46	0.001
PM2	-34.1	18.92	Intercept	6.46	2.11	3.07	0.002
			ADD	8.88	2.57	3.45	0.001
			BMI	2.23	1.21	1.85	0.065
FBM1	-37.4	18.74	Intercept	2.35	1.28	1.84	0.066
			ADD	6.45	1.94	3.33	0.001
FBM2	-35.3	17.20	Intercept	2.27	1.19	1.90	0.058
			ADD	6.78	2.11	3.21	0.001
			BMI	1.74	1.09	1.61	0.109
ADM1	-44.3	23.01	Intercept	5.83	2.71	2.15	0.032
			ADD	12.16	5.50	2.21	0.027
FCM1	-39.4	16.53	Intercept	3.48	1.56	2.22	0.026
			ADD	8.55	2.96	2.89	0.004
AWM1	-32.2	21.72	Intercept	2.10	1.48	1.42	0.155
			ADD	7.36	2.77	2.66	0.008
AWM2	-15.3	10.50	Intercept	5.04	3.36	1.50	0.134
			ADD	8.46	5.06	1.67	0.094
			Cancer	-3.16	2.91	-1.09	0.277
ACM1	-60.2	33.83	Intercept	-1.55	1.34	-1.16	0.248
			ADD	5.56	1.92	2.89	0.004
ACM2	-48.9	25.44	Intercept	0.49	1.37	0.36	0.722
			ADD	5.70	2.12	2.69	0.007
			Cancer	-3.13	2.51	-1.25	0.212
SM1	-45.3	20.37	Intercept	2.90	1.35	2.15	0.031
			ADD	8.32	2.81	2.97	0.003

***** *All continuous variables (ADD and BMI) are scaled as given in Table B1.*

REFERENCES

Anderson G, and VanLaerhoven S. 1996. Initial Studies on Insect Succession on Carrion in Southwestern British Columbia. J Forensic Sci 44(4):617-625.

Archer MS. 2004a. The effect of time after body discovery on the accuracy of retrospective weather station ambient temperature corrections in forensic entomology. J Forensic Sci 49(3):553-559.

Archer MS. 2004b. Rainfall and temperature effects on the decomposition rate of exposed neonatal remains. Sci & Justice 44(1):35-41.

Baccus JT, Becker HM, Simpson TR, and Manning RW. 2000. Mammals of the Freeman Ranch, Hays County, Texas. Freeman Ranch Publication Series. San Marcos, Texas: Southwest Texas State University. p 1-31.

Barnes PW, Liang SY, Jessup KE, Ruiseco LE, Phillips PL, and Reagan SJ. 2000. Soils, Topography and Vegetation of the Freeman Ranch. Freeman Ranch Publication Series. San Marcos, Texas: Soutwest Texas State University. p 1-29.

Bates D, Machler M, Bolker B, and Walker S. 2015. Fitting Linear Mixed-Effects Models Using lme4. J Stat Software 67(1):1-48.

Bates LN, and Wescott DJ. 2016. Comparison of decomposition rates between autopsied and non-autopsied human remains. Forensic Sci Int 261:93-100.

Campobasso CP, Di Vella G, and Introna F. 2001. Factors affecting decomposition and Diptera colonization. Forensic Sci Int 120(1-2):18-27.

Carter DO, Metcalf JL, Bibat A, and Knight R. 2015. Seasonal variation of postmortem microbial communities. Forensic Sci, Med, And Pathol 11(2):202-207.

Cobaugh KL, Schaeffer SM, and DeBruyn JM. 2015. Functional and Structural Succession of Soil Microbial Communities below Decomposing Human Cadavers. PLoS ONE 10(6):1-20.

Cross P, and Simmons T. 2010. The Influence of Penetrative Trauma on the Rate of Decomposition. J Forensic Sci 55(2):295-301.

Dabbs GR. 2010. Caution! All data are not created equal: The hazards of using National Weather Service data for calculating accumulated degree days. Forensic Sci Int 202(1-3):e49-e52.

Dabbs GR. 2015. How Should Forensic Anthropologists Correct National Weather Service Temperature Data for Use in Estimating the Postmortem Interval? J Forensic Sci 60(3):581-587.

Dabbs GR, Connor M, and Bytheway JA. 2016. Interobserver Reliability of the Total Body Score System for Quantifying Human Decomposition. J Forensic Sci 61(2):445-451.

DeVault TL, Rhodes OE, and Shivik JA. 2003. Scavenging by Vertebrates: Behavioral, Ecological, and Evolutionary Perspectives on an Important Energy Transfer Pathway in Terrestrial Ecosystems. Oikos 102(2):225-234.

Division of Nutrition Physical Activity and Obesity. 2014. Calculating BMI Using the English System. US. Department of Health & Human Services.

Division of Nutrition Physical Activity and Obesity. 2016. Defining Adult Overweight and Obesity. U.S. Department of Health & Human Services.

Dixon R. 2000. Climatology of the Freeman Ranch, Hays County, Texas. Freeman Ranch Publication Series. San Marcos, Texas: Southwest Texas State University. p 1-9.

Forensic Anthropology Center at Texas State. 2016. Whole Body Donation Information.

Galloway A, Birkby WH, Jones AM, Henry TE, and Parks BO. 1989. Decay rates of human remains in an arid environment. J Forensic Sci 34(3):607-616.

Gelman A, and Hill J. 2007. Data Analysis Using Regression and Multilevel/Hierarchical Models. New York: Cambridge University Press.

Gelman A, and Su Y-S. 2016. arm: Data Analysis Using Regression and Multilevel/Hierarchical Models. R package version 1.9-3 ed.

Gill-King H. 1997. Chemical and Ultrastructural Aspects of Decomposition. In: Haglund WD, and Sorg MH, editors. Forensic Taphonomy: The Postmortem Fate of Human Remains. Boca Raton: CRC Press.

Gleiber DS, Meckel LA, Siegert CC, McDaneld CP, Pyle JA, and Wescott DJ. 2017. Accumulated Decomposition Score (ADS): An Alternative Method to Total Body Score (TBS) for Quantifying Gross Morphological Changes Associated With Decomposition. American Academy of Forensic Sciences 69th Annual Scientific Meeting. New Orleans.

Hyde E, Haarmann D, Petrosino J, Lynne A, and Bucheli S. 2015. Initial insights into bacterial succession during human decomposition. Int J of Legal Med 129(3):661.

Johnson APBS, Wallman JFPD, and Archer MSPD. 2012. Experimental and Casework Validation of Ambient Temperature Corrections in Forensic Entomology. J Forensic Sci 57(1):215-221.

Klein AA. 2013. Vulture scavenging of pig remains at varying grave depths [Electronic thesis]. San Marcos: Texas State University. 55 p.

Liu W, Longnecker M, Tarone AM, and Tomberlin JK. 2016. Responses of Lucilia sericata (Diptera: Calliphoridae) to compounds from microbial decomposition of larval resources. Anim Behav 115:217-225.

Lopes de Carvalho LM, and Linhares AX. 2001. Seasonality of Insect Succession and Pig Carcass Decomposition in a Natural Forest Area in Southeastern Brazil. J Forensic Sci 46(3):604-608.

Mann RW, Bass WM, and Meadows L. 1990. Time since death and decomposition of the human body: variables and observations in case and experimental field studies. J Forensic Sci 35(1):103-111.

Marhoff SJ, Fahey P, Forbes SL, and Green H. 2016. Estimating post-mortem interval using accumulated degree-days and a degree of decomposition index in Australia: a validation study. Aust J Forensic Sci 48(1):24-36.

Matuszewski S, Konwerski S, Fratczak K, and Szafalowicz M. 2014. Effect of body mass and clothing on decomposition of pig carcasses. Int J of Legal Med 128:1039-1048.

McMaster GS, and Wilhelm W. 1997. Growing degree-days: one equation, two interpretations. Agric and Forest Meteorol 87(4):291-300.

Megyesi M, Nawrocki S, and Haskell N. 2005. Using Accumulated Degree-Days to Estimate the Postmortem Interval from Decomposed Human Remains. J Forensic Sci 50(3):1-9.

Micozzi M. 1986. Experimental study of postmortem change under field conditions: effects of freezing, thawing, and mechanical injury. J Forensic Sci 31(3):953-961.

Micozzi MS. 1997. Frozen Environments and Soft Tissue Preservation. In: Haglund WD, and Sorg MH, editors. Forensic Taphonomy: The Postmortem Fate of Human Remains. Boca Raton: CRC Press.

Mohr RM, and Tomberlin JK. 2014. Environmental Factors Affecting Early Carcass Attendance by Four Species of Blow Flies (Diptera: Calliphoridae) in Texas. J Med Entomol 51(3):702-708.

Myburgh J, L'Abbé EN, Steyn M, and Becker PJ. 2013. Estimating the postmortem interval (PMI) using accumulated degree-days (ADD) in a temperate region of South Africa. Forensic Sci Int 229(1-3):165-e1.

Parks CL. 2011. A Study of the Human Decomposition Sequence in Central Texas. J Forensic Sci 56(1):19-22.

Parsons HR. 2009. The postmortem interval a systematic study of pig decomposition in West Central Montana [Electronic thesis.]. Missoula: University of Montana.

Pechal JL, Tarone AM, Tomberlin JK, Benbow ME, and Crippen TL. 2014. Delayed insect access alters carrion decomposition and necrophagous insect community assembly. Ecosphere 5(4).

Reed HB. 1958. A Study of Dog Carcass Communities in Tennessee, with Special Reference to the Insects. Am Midl Naturalist 59(1):213-245.

Reeves NM. 2009. Taphonomic effects of vulture scavenging. J Forensic Sci 54(3):523-528.

Rhine S, and Dawson JE. 1998. Estimation of time since death in the southwestern United States. In: Bass W, and Reichs K, editors. Forensic Osteology: Advances in the Identification of Human Remains. 2 ed. Springfield: Charles C. Thomas. p 145-159.

Roberts LG, and Dabbs GR. 2015. A Taphonomic Study Exploring the Differences in Decomposition Rate and Manner between Frozen and Never Frozen Domestic Pigs (Sus scrofa). J Forensic Sci 60(3):588-594.

Roberts LG, Spencer JR, and Dabbs GR. 2017. The Effect of Body Mass on Outdoor Adult Human Decomposition. J Forensic Sci 62(5):1145-1150.

Rodriguez WC, and Bass WM. 1983. Insect activity and its relationship to decay rates of human cadavers in East Tennessee. J Forensic Sci 28(2):423-432.

Simmons T, Adlam RE, and Moffatt C. 2010a. Debugging Decomposition Data—Comparative Taphonomic Studies and the Influence of Insects and Carcass Size on Decomposition Rate. J Forensic Sci 55(1):8-13.

Simmons T, Cross PA, Adlam RE, and Moffatt C. 2010b. The Influence of Insects on Decomposition Rate in Buried and Surface Remains. J Forensic Sci 55(4):889-892.

Sincerbox SN, and DiGangi EA. 2018. Forensic Taphonomy and Ecology of North American Scavengers. London: Academic Press.

Spicka A, Johnson R, Bushing J, Higley LG, and Carter DO. 2011. Carcass mass can influence rate of decomposition and release of ninhydrin-reactive nitrogen into gravesoil. Forensic Sci Int 209:80-85.

Spradley MK, Hamilton MD, and Giordano A. 2012. Spatial patterning of vulture scavenged human remains. Forensic Sci Int 219:57-63.

Suckling JK. 2011. A longitudinal study on the outdoor human decomposition sequence in Central Texas [Electronic dissertations]. San Marcos: Texas State.

Sutherland A, Myburgh J, Steyn M, and Becker PJ. 2013. The effect of body size on the rate of decomposition in a temperate region of South Africa. Forensic Sci Int 231(1–3):257-262.

Tomberlin JK, Crippen TL, Tarone AM, Singh B, Adams K, Rezenom YH, Benbow ME, Flores M, Longnecker M, Pechal JL et al. . 2012. Interkingdom responses of flies to bacteria mediated by fly physiology and bacterial quorum sensing. Anim Behav 84(6):1449-1456.

Vass AA, Barshick S, Sega G, Caton J, Skeen J, Love J, and Synstelien J. 2002. Decomposition chemistry of human remains: A new methodology for determining the postmortem interval. J Forensic Sci 47(3):542-553.

Vass AA, Bass WM, Wolt JD, Foss JE, and Ammons JT. 1992. Time since death determinations of human cadavers using soil solution. J Forensic Sci 37(5):1236-1253.